1 Local glaciers record delayed peak Holocene warmth in South Greenland 2 Laura J. Larocca^a, Yarrow Axford^a, Anders A. Bjørk^b, G. Everett Lasher^{a,c}, & Jeremy P. Brooks^a 3 4 5 ^aDepartment of Earth and Planetary Sciences, Northwestern University, 2145 Sheridan Road, 6 Evanston, IL 60208 USA 7 8 ^bDepartment of Geography, University of Copenhagen, Øster Voldgade 10, 1350 Copenhagen K, 9 Denmark 10 11 ^cDepartment of Geology and Environmental Science, University of Pittsburgh, 4107 O'Hara 12 Street, Pittsburgh, PA 15260 USA 13 14 Keywords: Greenland, Holocene Thermal Maximum, lake sediments, mountain glaciers, paleotemperatures, Little Ice Age, equilibrium-line altitudes 15 16 17 **Abstract** 18 Local glaciers and ice caps (GICs) respond sensitively and quickly, on the scale of decades to 19 centuries, to climate variations. Continuous records of past fluctuations in GIC size provide 20 information on the timing and magnitude of Holocene climate shifts, and a longer-term perspective on 21st century glacier retreat. Although there is broad-scale agreement on 21 millennial-scale trends in Holocene climate variability and fluctuations in local GICs in 22 23 Greenland, regional variations are only loosely constrained. Here we present three Holocene proglacial lake sediment records from South Greenland, an area with abundant local glaciers but few Holocene-length paleoclimate records. In addition, we use geospatial analysis to model past equilibrium-line altitudes (ELAs) and thereby constrain the magnitude of ablation-season temperature change during the warmest and coolest periods of the Holocene. Physical and geochemical sedimentary characteristics show that two of the proglacial lakes continued to receive glacial meltwater input until ~7.3 and ~7.1 ka BP. The survival of local glaciers implies that South Greenland remained relatively cool, and that summer temperatures gradually warmed, but did not warm well beyond 1.2°C above present in the early Holocene. In the mid-Holocene, from ~7.1 to 5.5 ka BP, organic sedimentation at these two sites indicates that local glaciers became very small, or more likely melted away completely. The glaciers within the third lake's catchment melted away prior to ~5.2 ka BP, as sediments deposited earlier in the Holocene could not be dated at this site. We estimate that summer temperatures increased by at least 1.2-1.8°C above present by ~7.3-7.1 ka BP. Our results are consistent with other observations that suggest a north-to-south gradient in the timing of Holocene thermal maximum conditions, with southern Greenland experiencing a delayed warming relative to other regions in Greenland. As summer temperatures cooled in the Neoglacial, our records show that sustained glacier regrowth began ~3.1 ka BP with glaciers in the southernmost catchment, which at present, receive the most precipitation. In the other two catchments, which host smaller glaciers in a drier environment, regrowth began at ~1.3 and ~1.2 ka BP, the timing of which is in agreement with other glacial records from the Arctic Atlantic region. Local glaciers reached their maximum late Holocene extents during a cooler, second phase of the Little Ice Age (LIA) ~0.2-0.1 ka BP, that we estimate was at least 0.4-0.9°C cooler than present. Overall, these findings improve

24

25

26

27

28

29

30

31

32

33

34

35

36

37

38

39

40

41

42

43

44

understanding of the spatio-temporal dynamics of Holocene glacier and climate change in Greenland, potentially yielding valuable information about their future response.

48

49

50

51

52

53

54

55

56

57

58

59

60

61

62

63

64

65

66

67

68

47

46

1. Introduction

Existing paleoclimate studies in Greenland reveal consensus on millennial scale trends in Holocene climate, which generally corresponded with changes in Northern Hemisphere summer insolation and drove fluctuations in local glaciers and ice caps (GICs) peripheral to the Greenland Ice Sheet (GrIS) (Kelly and Lowell, 2009; Briner et al., 2016). In general, the early to middle Holocene was characterized by relatively warm temperatures and smaller than present or complete disappearance of GICs in Greenland. This was followed by cooling and GIC expansion in the late Holocene (Briner et al., 2016; Larsen et al., 2019). However, despite this broad-scale agreement, variability in the magnitude and timing of Holocene temperature trends and GIC fluctuations across Greenland remain uncertain. This hinders our understanding of the past sensitivity of ice masses to temperature change, with implications for forecasting Greenland's ongoing contribution to sea-level rise through the GrIS and the island's ~20,300 GICs (Rastner et al., 2012). Recent syntheses of temperature-sensitive proxy evidence from the western Arctic have established significant spatial and temporal asymmetries in peak Holocene warmth (Kaufman et al., 2004; Briner et al., 2016). In Greenland, proxy data suggests a north-to-south gradient in Holocene temperature trends with sites south of 66°N indicating a subdued and later period of Holocene maximum warmth, as well as a later onset of neoglacial cooling, relative to sites above 66°N (Briner et al., 2016). There is mounting evidence for especially strong warming over

northwest Greenland in the early Holocene (Axford et al., 2019; McFarlin et al., 2018).

Temperature inferences from the Agassiz Ice Cap on Ellesmere Island adjacent to northwest Greenland indicate an early Holocene thermal maximum (HTM) that was several degrees warmer than the preindustrial late Holocene (Lecavalier et al., 2017). Modeling results integrating the large inferred warming over the northern sector of the GrIS show a ~1.4 m sealevel equivalent increase in ice sheet mass loss during the last deglaciation, from ~18 ka BP (Lecavalier et al., 2017). In contrast, paleoclimate data from southernmost Greenland is sparse. Only a few reconstructions infer temperature changes spanning the early to late Holocene (Kaplan et al., 2002; Andresen et al., 2004; Wooller et al., 2004; Fréchette and Vernal, 2009; Massa et al., 2012; Gajewski, 2015) (Fig. 1) and to date, evidence capturing the regional expression of the HTM in South Greenland is not in good agreement. Moreover, sensitivity tests investigating significant data-model misfits in relative sea-level histories at some locations in southern Greenland indicate that HTM forcing or response to this forcing may be over-estimated (Woodroffe et al., 2014). These results highlight the implications of spatial variability in the timing and magnitude of peak Holocene warmth to the understanding of cryosphere evolution. Small mountain glaciers are exceptionally sensitive and respond rapidly to modest climate changes (Oerlemans, 2005). Historical air photo and satellite observations of local, landterminating glaciers across Greenland from the 20th and 21st centuries have confirmed this sensitivity, and have documented frontal change in response to both warming and cooling on a decadal scale (Bjørk et al., 2012, 2017; Leclercq et al., 2012). Beyond instrumental timescales, analysis of glacial lake sediments have allowed for continuous reconstructions of local GIC fluctuations through the Holocene in Greenland, and have expanded our knowledge of regional Holocene climate variability and GIC sensitivity on longer time-scales (e.g, Lowell et al., 2013; Levy et al., 2014; Balascio et al., 2015; Larsen et al., 2017; Schweinberg et al., 2017, 2018,

69

70

71

72

73

74

75

76

77

78

79

80

81

82

83

84

85

86

87

88

89

90

2019; van der Bilt et al., 2018; Larsen et al., 2019; Axford et al., 2019). However, to our knowledge, no studies have determined whether GICs survived the warmth of the HTM in southernmost Greenland, in contrast with other regions in Greenland (e.g., Larsen et al., 2019). In this study, we present three continuous lacustrine records of local glacier fluctuations in South Greenland (Fig. 1). In addition, we infer changes in past glacier extents and equilibrium-line altitudes (ELAs) from lake sediments and geomorphological evidence to model past summer temperature conditions relative to present for multiple time slices. Overall, we aim to constrain the timing of the warmest and coldest periods of the Holocene in South Greenland, as well as the amplitudes of the associated temperature changes.

2. Study Area

2.1. Geographical Setting and Climate

The glacial lakes Quvnerit, Alakariqssoq, and Uunartoq (informal names) are located in the Kujalleq region which encompasses the southernmost part of Greenland (Fig. 1). The region is highly mountainous with many steep-sided coastal fjords neighboring the North Atlantic and Labrador Sea. The 6500 km² Julianehåb Ice Cap, which is confluent with the southern sector of the GrIS, is situated on a high elevation bedrock plateau in the east (Fig. 1). The 100 km wide, lower lying Qassimiut lobe, a climatically sensitive part of the southern GrIS, is located to the west (Larsen et al., 2016) (Fig. 1). A basal limiting age from a lacustrine record suggests the outer coast of South Greenland was ice free by 14.1 ka BP (Andresen et al., 2004; Björck et al., 2002), and beryllium-10 surface exposure ages suggest that this sector of the ice sheet first retreated within its late Holocene maximum extent, beginning 11.1 to 10.6 ka BP (Carlson et al., 2014). Presently, the land west and southwest of the Julianehåb Ice Cap hosts approximately 900

local GICs, mostly on north-oriented slopes. These GICs have an average area of ~0.6 km², and an average minimum and maximum elevation of ~840 and ~1240 m above sea level (a.s.l.) respectively (Raup et al., 2007). Geomorphological evidence of past GIC extent including historical/Little Ice Age (LIA) trimlines and moraines are visible in the landscape.

115

116

117

118

119

120

121

122

123

124

125

126

127

128

129

130

131

132

133

134

The modern climate of the region is low Arctic and is modulated by its close proximity to the Labrador Sea and North Atlantic currents. South of Kap Farvel, the cold, low salinity, East Greenland current (EGC) converges with the Irminger current (IC), a westward-moving, warm, saline current derived from Atlantic waters. These polar and Atlantic waters join to form the West Greenland current (WGC), which flows northward along Greenland's west coast (Fig. 1). Due to this maritime influence, the annual variability in temperature at Kap Farvel is less than ~10°C, and climate is wet and windy, with a large precipitation gradient across a small area (Cappelen et al., 2001). At Qaqortoq weather station, (Fig. 1; 40 and 55 km northwest of Alakarigssog and Uunartog lakes, respectively) the mean annual temperature is 0.6°C, and the mean summer (June, July, August) temperature is 6.5°C. Mean annual accumulated precipitation is 858 mm, and winter (December, January, February) precipitation is 181 mm. At Prins Christian Sund, 175 km southeast of Qagortog and 38 km northeast of Quvnerit Lake, mean annual temperature is 0.7°C, mean summer temperature is 5.8°C, mean annual accumulated precipitation is 2474 mm, and winter precipitation is 759 mm. At Kap Farvel, ~22 km southwest of Quvnerit Lake, annual precipitation is even higher, up to 3000 mm per year (meteorological data were recorded during the period 1961-90) (Cappelen et al., 2001).

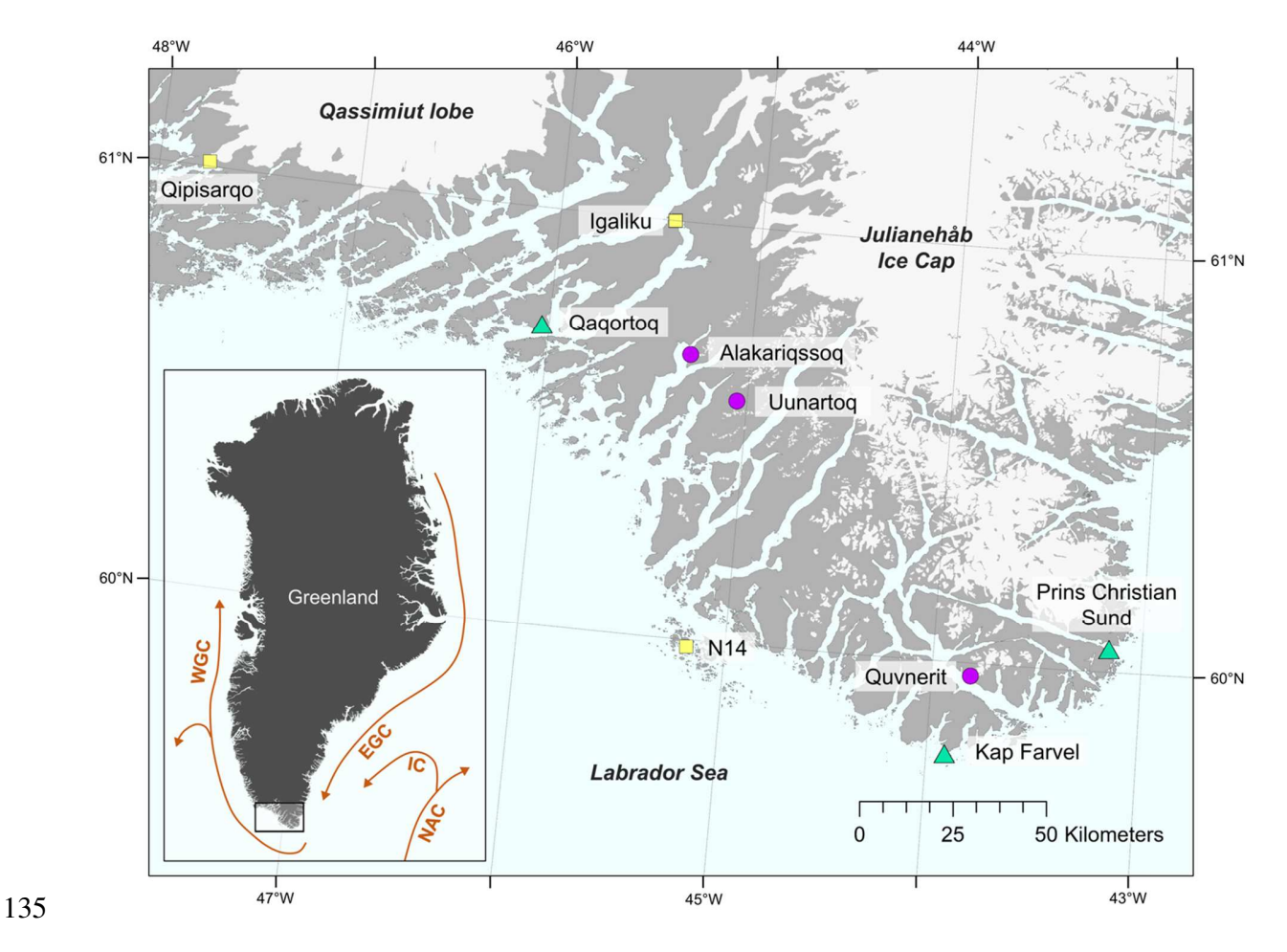


Figure 1. Major ocean currents and locations discussed in the text. Overview map of the study region, including weather stations (green triangles), glacial lake sites described in this study (purple circles), and other published paleoclimate records (yellow squares, Qipisarqo: Kaplan et al., 2002; Wooller et al., 2004; Frechétte and de Vernal, 2009, Igaliku: Massa et al., 2012, and N14: Andresen et al., 2004). Inset shows the study region within Greenland and major ocean currents: West Greenland Current (WGC), Irminger Current (IC), East Greenland Current (EGC), and North Atlantic Current (NAC).

2.2. Study Sites

Quvnerit Lake is a small (~0.05 km², 15 m maximum depth) glacial lake, situated at 125 m a.s.l. and above the local marine limit. The lake is ~22 km northeast of Kap Farvel and the open waters of the North Atlantic (Fig. 1). At present, meltwater from two mountain glaciers (the larger ~3.0 km² in size and located between ~600-1120 m a.s.l., and the smaller ~0.3 km² in size and located between ~600-920 m a.s.l.) flows through an upper, larger (~0.1 km²) glacial lake before reaching Ouvnerit (Fig. 2A). The smaller glacier is located completely inside the lake's ~9.0 km² catchment, whereas the larger glacier is only partially within Quvnerit's catchment. Two sediment cores were investigated (Table 1). 18-QUV-N2 is a 437 cm core retrieved at 13.6 m water depth (N 59°58.223, W 43°48.823), which captured the sediment-water interface but with some disturbance of it (muddy water above during core recovery). 18-QUV-N5 was recovered at 11.85 m water depth (N 59°58.192, W 43°48.945), with the goal of obtaining a deeper record; the top of its 325-cm sediment record begins at 240 cm below the sediment-water interface, and the core ended in refusal. Together, these overlapping cores capture ~5.6 meters of sediment, which based on sonar data, should cover the lake's entire sediment package (Fig. 2A). Alakarigssog Lake is a small (~0.1 km², 8 m maximum depth) glacial lake, situated at 230 m a.s.l. (Fig. 1). Presently, the lake receives meltwater from four small (~1.1 km² in total, representing ~12% of the ~9.1 km² catchment area), north-facing, high elevation (~920-1450 m a.s.l.) mountain glaciers (Fig. 2B). Two sediment cores were investigated (Table 1). 18-ALA-N1 is a 135 cm core retrieved at 7.65 m water depth (N 60°40.907, W 45°17.705). ~15 cm of sand was lost from the bottom of the core. 18-ALA-U1 is a 135 cm core retrieved at 7.4 m water depth, and ~1 m south of N1. The sediment-water interface was captured in core U1 and was

undisturbed. According to sonar data the entire sediment package was obtained (Fig. 2B).

145

146

147

148

149

150

151

152

153

154

155

156

157

158

159

160

161

162

163

164

165

Uunartoq Lake is a small (~0.02 km², 10 m maximum depth) glacial lake, situated at 480 m a.s.l. (Fig. 1). Presently, the lake receives meltwater from several small (~0.9 km² in total, representing ~13% of the ~6.8 km² catchment area), north-facing mountain glaciers located between ~850-1370 m a.s.l. Two terminal moraine deposits are visible within the catchment (herein referred to as M1 and M2) (Fig. 2C). M1, located ~0.2 km southeast of the lake, is a pre-LIA, large terminal moraine lushly covered in dwarf birth and heaths. M2 is free of vegetation and is located ~1.8 km southeast of Uunartoq between two very small upstream glacial lakes, and presumably marks the maximum historical extent. Two sediment cores were investigated (Table 1). 18-UUN-N2 is a 93 cm core retrieved at 9.8 m water depth (N 60°34.927, W 45°03.042). The upper ~11 cm of sediment, and thus the sediment-water interface was not captured. 18-UUN-U3 is a 91 cm core retrieved at 9.8 m water depth and ~1 m northeast of N2, with the sediment-water interface intact. Only the first 50 cm of U3 was analyzed as it is suspected that younger material was sucked into the bottom of the core tube during extraction. Based on sonar data, the two cores together cover the full sediment package, which is likely underlain by glacial till (Fig. 2C).

Vegetation at our study sites is shrub tundra with dwarf birch and heaths. Felsic magmatic bedrock of the Julianehåb igneous complex surrounds Alakariqssoq and Uunartoq lakes, and Quvnerit Lake is underlain by Paleoproterozoic metasedimentary and metavolcanic rocks (Steenfelt et al., 2016).

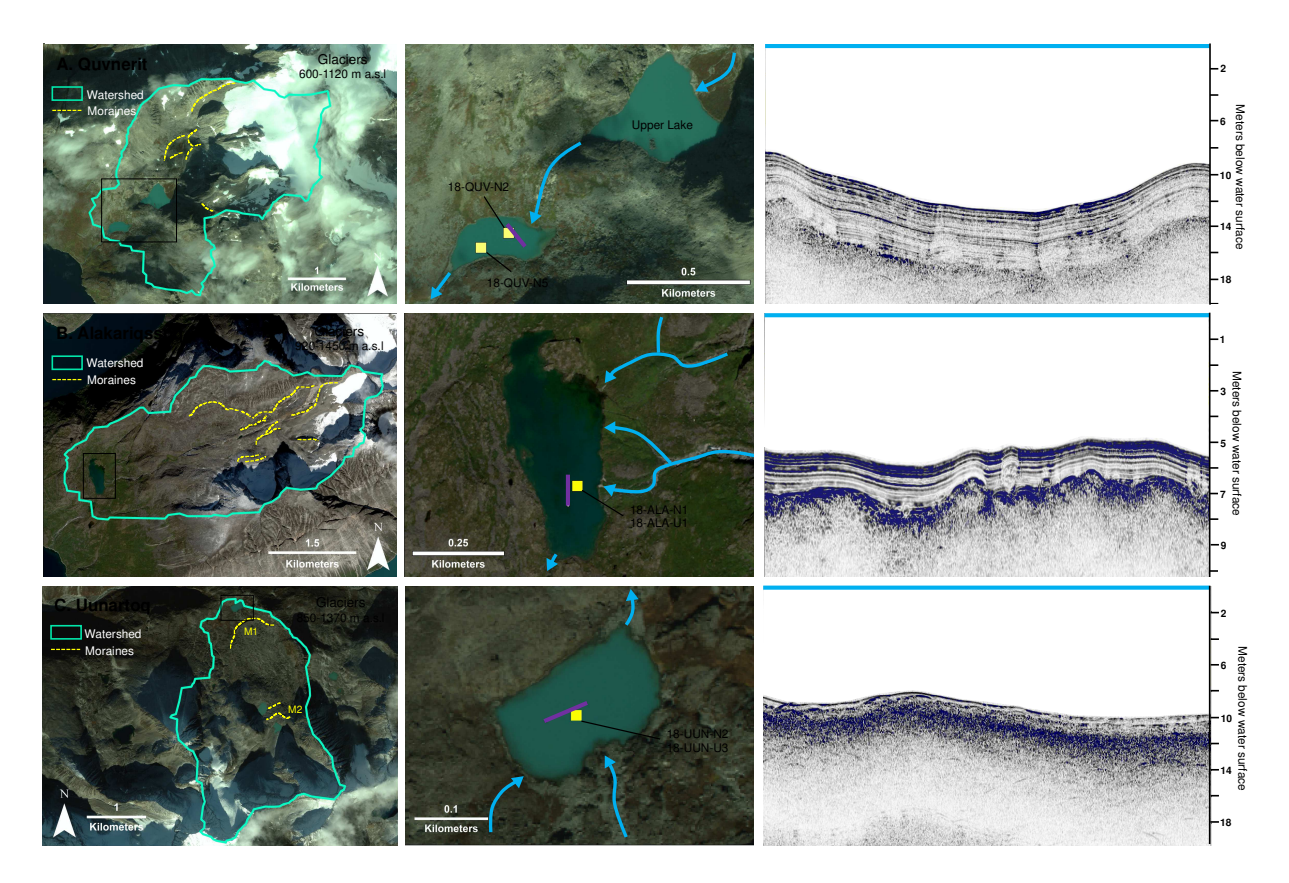


Figure 2. Map view of proglacial lakes and local glaciers analyzed in this study: **A.** Quvnerit, **B.** Alakariqssoq, and **C.** Uunartoq lake. Left panels show watersheds denoted by cyan polygons, and glacial moraines by yellow dashed lines. Two sets of moraines of different ages are preserved in the Uunartoq lake catchment, with M1 being pre-LIA and M2 LIA/historical. In middle panels, major inlets and outlets are denoted by solid blue lines, coring locations by yellow squares, and locations of the sonar image transects (right panels) are denoted by purple lines. Right panels show sediment stratigraphy and thickness from acoustic sub-bottom profiling. Sediment package thickness is on average ~5 m, ~1.5 m, and ~1 m respectively. The brown lines show the base of lacustrine sediments at each site and the blue line marks the water surface. Strong reflections mark boundaries between sediment with dissimilar characteristics. 2012-2016 late summer Worldview-2 imagery copyright 2019 Digital Globe, Inc.

3. Methods

199

200

201

202

203

204

205

206

207

208

209

210

211

212

213

214

215

216

217

218

219

220

221

3.1. Reconstructing past glacier-climate change

We combine glacial lake sediment analyses with geospatial analyses to determine the timing of past glacier fluctuations over the Holocene, as well as the corresponding summer temperature change required to cause these fluctuations. At the ice-bed interface, the erosional capability of temperate glaciers by plucking, abrasion, and crushing increases with glacier size; accordingly, the transport of clastic sediments into proglacial lakes is higher when a larger glacier is present (Jansson et al., 2005). Thus, accumulated sediment may be used to infer change in glacier size by examining the variability in clastic sediment input (Nesje et al., 2000; Dahl et al., 2003; Balascio et al., 2015). We interpret sediments dominated by minerogenic, fine-grained (silty-clay) material as indicative of glacier presence, whereas sediment higher in organic material (gyttja) are indicative of a glacier reduced in size relative to today or of no glacier in the catchment. Based on the configuration of glaciers within the catchments, Alakariqssoq and Uunartoq lakes would continue to receive glacial meltwater until the glaciers in their catchments completely melted away. Quvnerit Lake would receive glacial meltwater until the larger upstream glacier becomes very small in size and recedes behind a topographic barrier. These onoff threshold-style records essentially timestamp when the glaciers are at or near the threshold, and allow for a corresponding constraint on glacier extent and ELA to be established (Dahl et al., 2003). Glacier mass balance and ELA are largely dependent on two main factors: snow accumulation, and summer season ablation which is generally controlled by mean melt-season

temperature (e.g., Nesje 1989; Lowell, 2000; Dahl et al., 2003; Oerlemans, 2001, 2005).

However, in general, glaciers are more sensitive to changes in melt-season temperature than to

other climatic changes (e.g., Oerlemans, 2001). Several recent observational studies show a robust relationship between fluctuations in Greenlandic glaciers and summer air temperature over the past century (Bjørk et al., 2012; Leclercq et al., 2012). We infer minimum HTM and LIA ablation-season temperature anomalies relative to present by comparing the elevation of modern (2016-2019) glacier ELAs (i.e. snowlines) with Holocene paleo-ELA estimates (which we establish through lake sediment properties and geomorphological evidence of past glacier extent). We make the assumption that precipitation remained constant through the Holocene, such that the temperature change (ΔT) responsible for an ELA elevation shift (ΔELA) can be approximated via the atmospheric lapse rate: $\Delta T = \Delta ELA * \Gamma$, where Γ is the atmospheric lapse rate for the region of interest (i.e. ~0.68°C/100 meters on average in modern-day Greenland) (e.g., Nesje et al., 1991; Dahl and Nesje, 1992; Fausto et al., 2009). This in turn yields quantitative constraints on Holocene temperature extremes, albeit with significant uncertainties owing to the method's assumptions. In the following sections, we provide further methodological detail on the lake sediment and geospatial analyses.

3.2. Coring and field methods

The three proglacial lakes were cored in summer 2018 using a Nesje percussion piston corer (Nesje, 1992), and a piston-free Universal check-valve percussion corer to capture the intact sediment-water interface. Two adjacent cores are reported from each lake, to assess replicability of the records, and in some cases, to extend the record beyond the length of a single core (Table 1). A Lowrance HDS-7 was used to measure lake depth, and an EdgeTech 3100-P sub-bottom profiling system equipped with a SB-424 towfish was used to gauge the sediment package thickness and stratigraphy, and to select coring locations at each lake (Fig. 2). The

towfish was towed at 1-2 knots, ~1 meter below the water surface. Sonar data was collected with a 4-24 kHz pulse bandwidth and 5 millisecond pulse length and processed in real-time during collection using EdgeTech's DISCOVER software. Coring areas were selected based on the sediment package thickness, intactness of the stratigraphy, flatness of the bottom, and characteristics of the surrounding landscape. Areas with disturbed sediment, trapped gas, boulders, and/or steep slopes were avoided. Based on field observations of the surrounding landscapes, other processes that could introduce clastic sediments at the coring sites, such as mass wasting via steep surrounding slopes, and thick erodible soil cover, are limited.

Table 1. Lake sediment core metadata.

Lake Name	Lake elevation (m a.s.l.)	Core ID	Latitude	Longitude	Water depth (m)	Sediment depth at top of core (cm)	Core length (cm)	Coring device
Quvnerit	125	18-QUV-N2	N 59°58.223	W 43°48.823	13.6	0	437	Nesje
Quvnerit	125	18-QUV-N5	N 59°58.192	W 43°48.945	11.85	240	325	Nesje
Alakariqssoq	230	18-ALA-U1	N 60°40.907	W 45°17.705	7.4	0	135	Universal
Alakariqssoq	230	18-ALA-N1	N 60°40.907	W 45°17.705	7.65	~0	135	Nesje
Uunartoq	480	18-UUN-U3	N 60°34.927	W 45°03.042	9.8	0	*91	Universal
Uunartoq	480	18-UUN-N2	N 60°34.927	W 45°03.042	9.8	~11	93	Nesje

^{*}Only the top 50 cm were analyzed on core 18-UUN-U3 (see text for further information).

3.3. Sediment characterization

To distinguish minerogenic-rich glacial sediments from organic-rich non-glacial sediments, as well as to determine more fine-scale, subtle variations in minerogenic input reflective of changes in glacier size, we measured magnetic susceptibility (MS), visible color reflectance, and major element abundance on freshly split cores every 2 mm using a Geotek MSCL-S. The instrument is equipped with a Bartington point sensor (MS2E), a Konica Minola CM-700d

spectrophotometer, and an Olympus DELTA Professional X-Ray Florescence (XRF) spectrometer. The XRF spectrometer is configured with a 40kV Rhodium anode X-ray tube and measurements were made with a dwell time of 30 seconds, with the core surface covered in a 4µm Ultralene film. To determine sediment organic matter content, we measured loss-onignition (LOI) at 3 cm intervals by combustion of dried 1-cm³ bulk sediment samples at 550°C for 4 hours (e.g., Heiri et al., 2001).

In order to characterize the leading modes of variability in the measured geochemical and physical properties, principal component analysis (PCA) was performed in R using the Vegan Package (version 2.5-2). LOI, MS, and nine elements from the elemental abundance data were included in the PCA (Ti, Si, Ca, Al, Fe, K, Mn, Rb, Sr) and were selected based on their abundance in the local bedrock, and their usage in prior studies to infer changes in minerogenic input and glacial activity (e.g., Balascio et al., 2015; Larsen et al., 2017; Schweinsberg et al., 2017, 2018, 2019). Prior to the analysis, the higher resolution datasets (XRF elemental data and MS) were down sampled by interpolation to the lowest resolution dataset, LOI (at every 3 cm).

3.4. Chronology

We base core chronologies on aquatic macrofossils (n=28) and aquatic invertebrate remains (chironomid head capsules and cladocera ephippia; n=1) which were picked and cleaned with deionized water. Accelerator Mass Spectrometry (AMS) 14 C ages were determined at Woods Hole Oceanographic Institution's National Ocean Sciences Accelerator Mass Spectrometry Facility (NOSAMS) and calibrated using CALIB version 7.1 and the IntCal13 calibration curve (Reimer et al., 2013; Stuiver et al., 2017). Calibrated ages are reported as the midpoint of the 2σ range, \pm

half of the 2σ range (Table 2). To our knowledge, hardwater effects in lacustrine organic materials have never been reported from comparable crystalline bedrock terranes in Greenland.

Age-depth models (Table 2 and Fig. S1) were generated for all lake cores (except core N2 from Uunartoq lake which has two radiocarbon ages and were only used to correlate core N2 to U3) using the Bacon age modeling package in R, version 2.2 (Blaauw and Christen, 2011), and the mean was used for data interpretation. The chronology for Quvnerit lake core N2 was established from radiocarbon ages of six aquatic moss samples. We excluded the erroneously old sample (at 7-8 cm) from the age-depth model. Radiocarbon ages of three aquatic moss samples were used in the age-depth model for the Quvnerit lake core N5. For Alakariqssoq lake core U1 and N1, radiocarbon ages of six and four aquatic moss samples, respectively, were used in the age-depth model. Six samples (omitting the inverted age from 38-39 cm) were used in the age-depth model for Uunartoq lake core U3. The top of cores collected with the sediment-water interface intact (i.e. QUV-N2, ALA-U1, and UUN-U3) were set to the year of collection (i.e. –68 cal yrs BP). For cores that did not capture the sediment-water interface (i.e. QUV-N5 and ALA-N1), the age-depth models were set to begin with the sample of the youngest ¹⁴C age. Age-depth models were not extended past the oldest ¹⁴C ages in any case.

Table 2. Radiocarbon ages from lakes Quvnerit (QUV), Alakariqssoq (ALA), and Uunartoq (UUN).

Core	Depth in sediment (cm)	Lab ID	Material Dated	Fraction Modern	$\delta^{13}C$	Radiocarbon Age (¹⁴ C yr BP)	Calibrated Age (cal yr BP)
*18-QUV-N2	7-8	OS-144995	Aquatic moss	0.7671±0.0022	-23.46	2130±25	2150±145
18-QUV-N2	48-49	OS-146797	Aquatic moss	0.8471±0.0116	Not measured	1330±110	1250±270
18-QUV-N2	121-122	OS-144996	Aquatic moss	0.7617±0.0021	-22.58	2190±20	2310±165
18-QUV-N2	221-222	OS-145236	Aquatic moss	0.6017±0.0017	-25.44	4080±25	4625±175

18-QUV-N2	279-280	OS-144997	Aquatic moss	0.5282±0.0022	-24.32	5130±35	5870±115
18-QUV-N2	329	OS-146798	Aquatic moss	0.4356±0.0073	-24.25	6680±130	7555±235
18-QUV-N2	385	OS-144998	Aquatic moss	0.3757±0.0020	-22.02	7860±40	8740±190
18-QUV-N5	242-243	OS-144999	Aquatic moss	0.6040±0.0032	-24.25	4050±40	4610±190
18-QUV-N5	342	OS-145237	Aquatic moss	0.4760±0.0017	-25.66	5960±30	6790±95
18-QUV-N5	475	OS-145238	Aquatic moss	0.3489±0.0017	-17.53	8460±40	9485±50
18-ALA-U1	4-5	OS-146807	Aquatic moss	0.9802±0.0020	-23.49	160±15	145±140
18-ALA-U1	25-26	OS-146808	Aquatic moss	0.8880±0.0019	-29.52	955±15	860±65
18-ALA-U1	35-36	OS-146809	Aquatic moss	0.8125±0.0023	-23.81	1670±25	1610±80
18-ALA-U1	95-96	OS-146810	Aquatic moss	0.4075±0.0021	-26.67	7210±40	8055±100
18-ALA-U1	108-109	OS-146811	Aquatic moss	0.3212±0.0024	-27.63	9120±60	10340±145
18-ALA-U1	118-119	OS-146812	Aquatic moss	0.3096±0.0023	-22.73	9420±60	10755±310
18-ALA-N1	13-14	OS-146788	Aquatic moss	0.8755±0.0118	Not measured	1070±110	1010±250
18-ALA-N1	30	OS-146804	Aquatic moss	0.8114±0.0018	-23.60	1680±20	1610±75
18-ALA-N1	92	OS-146805	Aquatic moss	0.4718±0.0020	-21.42	6030±35	6875±95
18-ALA-N1	129	OS-146806	Aquatic moss	0.3097±0.0024	-23.55	9420±65	10755±315
18-UUN-U3	14-15	OS-147678	Aquatic moss	0.8312±0.0102	Not measured	1490±100	1400±210
18-UUN-U3	17	OS-147806	Plant material/aquatic moss	0.8043±0.0094	-23.36	1750±95	1650±235
18-UUN-U3	24.5	OS-147683	Aquatic moss	0.7238±0.0017	-20.94	2600±20	2740±15
18-UUN-U3	26-27	OS-147684	Aquatic moss	0.7148±0.0015	-24.82	2700±15	2805±40
18-UUN-U3	31-32	OS-147698	Aquatic moss	0.6618±0.0016	-24.96	3320±20	3545±65
*18-UUN-U3	38-39	OS-147807	Aquatic moss	0.7854±0.0101	-23.73	1940±100	1880±260
18-UUN-U3	39-40	OS-151617	Aquatic invertebrate remains	0.5659±0.0050	-18.93	4570±70	5225±245
18-UUN-N2	12-13	OS-147676	Aquatic moss	0.6877±0.0092	-23.55	3010±110	3165±280
18-UUN-N2	14-15.5	OS-147677	Plant material/aquatic moss	0.6693±0.0081	-25.12	3230±95	3455±230

moss moss *Ages not included in age models (see text for further information). Calibrated ages are reported as midpoint of the 2σ range $\pm 1/2$ of 2σ range.

3.5. Geospatial (ELA) analysis

304

305

Modern ELAs (i.e. snowlines) were assessed by averaging late summer (July, August, and/or September) snowlines across several time-slices between the years 2016-2019, since the extents of present-day glaciers may not be in equilibrium with current climate. Snowline elevations were constrained by digitizing the line in which white snow meets glacial ice from cloud-free Landsat and Sentinel imagery using the Google Earth Engine Digitisation Tool (GEEDiT) (Lea, 2018). The ArcticDEM 2 m resolution mosaic (Porter et al., 2018) was used to extract the mean snowline elevation. In general, we found that average modern snowlines were somewhat higher in elevation than the calculated ELA (the AAR ELA calculated using the modern glacier extents), supporting our inference that the glacier's current extents do not yet reflect present-day summer temperatures (Table 3).

We estimate the LIA temperature depression by comparing present snowlines with modeled LIA ELAs. Paleoglacier LIA ELAs were modeled using two ArcGIS toolboxes (Pellitero et al., 2015, 2016). The first toolbox, called GlaRe, reconstructs the 3D surface of paleoglaciers using glacier physics and evidence of past glacial extent. We establish past glacier extent through proglacial lake records and geomorphological evidence of the maximum historical extent via moraines and trimlines. In cases where there are multiple historical moraines, we use the outermost moraines for our reconstructions. The GlaRe toolbox generates ice thickness from bed topography, along user-defined flowlines, by using a numerical approach that is based on an iterative solution to the perfect plasticity assumption for ice rheology. Along with the paleoglacier extent information, the tool allows for three additional user-defined inputs: the basal shear stress, shape factor (i.e. lateral drag), and interpolation procedure. We adjusted the basal shear stress input along flowlines to reconstruct paleoglacier surfaces with thicknesses that best fit LIA trimline height (Table S2). To extrapolate the generated ice thickness values

along the glacier's flowline and to generate the 3D glacier surface, we used the Topo to Raster and Kriging interpolation procedures. GlaRe also includes a toolset for instances in which part of the paleoglacier bed is presently covered by ice, which is the case for all the glaciers we reconstructed in South Greenland. The additional tool was employed before the aforementioned procedures, to estimate the subglacial bed topography, based on an inversion of an ice surface profile model by Benn and Hulton (2010) (Pellitero et al., 2016). We used the ArcticDEM 2 m resolution mosaic (Porter et al., 2018) for the modern ice surfaces in our analyses.

Utilizing the modelled surface output from GlaRe, we used a second toolbox developed for automated calculation of glacier ELAs (Pellitero et al., 2015) to estimate the LIA steady-state ELA (which assumes the glacier was in equilibrium with climate). We use the Accumulation-Area Ratio (AAR) method which is based upon the assumption that the accumulation area of a glacier represents a fixed fraction of the glacier's total area (Benn and Lehmkuhl, 2000), and can be calculated as: $AAR = A_c /(A_c + A_b)$, where A_c is the accumulation area, and $(A_c + A_b)$ is the total area (Meier, 1962). This method does not take the mass-balance gradient into account. The AAR fraction is specific to glacier type and regional climate. We used an AAR of 0.67, a common value for high-latitude alpine glaciers in equilibrium (Gross et al., 1976; Braithwaite and Muller, 1980).

Glacier disappearance occurs after the ELA rises above the highest point on a glacier (causing a loss of the entire accumulation area). Thus, for glaciers that lie completely within the lake's catchment (Alakariqssoq and Uunartoq) and where our sediment records indicate that glaciers completely disappeared during the middle Holocene, we treat the highest elevation on the extant glaciers as the minimum HTM ELA. Anderson et al. (2019) demonstrates a recent precedent for our approach and showed that the difference between the modern ELA and the

highest local topography, or the elevation change in which there would be a loss of accumulation area (termed the critical ELA change, ΔELA^{crit}), exerts a first-order control on the timing of glacier inception and disappearance. Accordingly, the critical ELA change yields an estimate of the temperature rise relative to modern that is needed to melt away the glacier completely, and thus a minimum bound on local ablation-season temperature for the period of glacier disappearance (which we define as the local HTM). In one case (the larger glacier only partially inside Quvnerit's watershed, i.e. Quvnerit 1), and for which we therefore can't confirm complete disappearance during the HTM we report two ΔELA-derived summer temperature estimates. The first compares the present snowline with the highest elevation on the present-day glacier within Quvnerit's watershed, as this is the elevation at which no glacially derived sediment would enter the lake. The second compares the present snowline with the highest point on the present-day glacier, and thus yields an estimate of the warming associated with complete disappearance of the glacier.

We do not correct our reconstructed ELAs for glacio-isostatic land uplift. Following deglaciation, relative sea level (RSL) fell rapidly from a local marine limit of ~50 m and reached present sea level by the early Holocene, ~9.5 ka BP. RSL remained below present (by up to ~10 m) before rising to present in the last 2000 years (Woodroffe et al., 2014). Thus, we suggest that the amount of uplift within the Holocene in our study region is small enough to have a negligible effect on our reconstructed ELAs and ablation season temperature estimates.

Our estimates of summer temperature change, based upon the difference between the modern snowline and modeled paleo-ELAs, assume no change in precipitation (i.e. accumulation). However, we acknowledge the likely possibility that the amount of precipitation and precipitation seasonality (impacting the amount of precipitation falling during the

accumulation (i.e. winter) season) changed during the Holocene, especially given South Greenland's proximity to North Atlantic moisture sources. Although terrestrial reconstructions of Holocene hydroclimate in Greenland are still sparse, studies have suggested that both changes in local evaporation from nearby seas via changes in ocean surface conditions such as sea-ice cover and ocean heat content, and meridional moisture gradients which effect moisture transport from lower latitudes, regulate high-latitude precipitation change (Thomas et al., 2016; 2018). Moreover, warmer temperatures, and associated reductions in sea-ice cover have been shown to be particularly important to winter season precipitation, with enhanced early winter local surface evaporation causing large increases in early winter snowfall (Bintanja and Selten, 2014).

This significant uncertainty bolsters our interpretation of estimated temperature anomalies as minimum constraints. During the middle Holocene, alongside warming, there is evidence that southernmost Greenland became more humid between 8-5 ka BP (e.g., Andresen et al, 2004). In addition, minimum sea-ice cover in the eastern Labrador Sea, is recorded in the middle Holocene between 7-6 ka BP (de Vernal et al., 2013). Higher precipitation during the middle Holocene HTM would render our temperature estimates true minimum bounds, as an increase in precipitation could have counteracted some ice loss due to warming and thus partially mitigated rising ELAs. Nonetheless, studies of land terminating GICs have shown that quite a large increase in precipitation (between 30-40%) is needed to counterbalance the effects of a 1°C warming (e.g., Oerlemans, 2001; Alley, 2003). Similarly, if precipitation was reduced during the relatively cold LIA, our LIA temperature estimates are also a true minimum on cooling, as reduced precipitation would have a negative effect on glacier mass balance and elevate the ELA. Thus, reporting our estimates as minimum constraints on temperature anomalies helps account for uncertainties regarding past precipitation.

4. Results and site-specific interpretations

4.1. Principal component analysis

PCA was used to characterize shared patterns of variability between the physical and geochemical sedimentary parameters at each lake site, and ultimately to further distinguish minerogenic-rich, glacially derived sediment from organic-rich sediment. The PCA biplots (Fig. S2-4) for the three lake records indicate that the geochemical elements are strongly positively correlated with one another, positively correlated with MS, and strongly negatively correlated with LOI. The first principal component (PC1) explains 76% and 63% of the total variance in the Quvnerit lake cores N2 and N5, respectively; 90% and 80% in the Alakariqssoq lake cores U1 and N1, respectively; and 85% and 92% in the Uunartoq lake cores U3 and N2, respectively. These results suggest that our multivariate datasets have a strong common signal and support the use of the PC1 scores (Fig. 7) to summarize changes in minerogenic input, and thus glacier activity in the catchments over time. Below, we describe detailed results from each lake site.

4.2. Quvnerit

Core 18-QUV-N2 is subdivided into four units (Fig. 3). The core 18-QUV-N5 contains three comparable units, albeit with depths in the core offset relative to 18-QUV-N2 because core N5 bypassed the upper 240 cm of sediment (Fig. 3). The lower unit (D, core N2: 437-320 cm; core N5: 565-359 cm total depth below the sediment-water interface) is comprised of laminated to massive silty-clays and sands with a few moss layers. The unit has low organic matter content (1.5-4%), high Ti concentration, and high MS. However, there is an unexplained dip in MS from 415-380 cm in core N5. PC1 scores reflect minerogenic input into the lake and show a gradual

declining trend through the unit in core N5. Unit D is interpreted as representing a period with glacial meltwater input. Unit C (core N2: 320-260 cm; core N5: 359-285 cm total sediment depth) is a relatively organic-rich gyttja unit comprised of laminated aquatic moss layers and is brown in color. Organic matter content is relatively high, between ~4-6% in core N2 and ~2.5-5.5% in core N5. Ti concentration and MS are relatively low. PC1 scores reflect more organic rich sedimentation. Unit C is interpreted as a period with no glacial meltwater input (i.e. as part of the larger glacier is outside the lake's catchment, the glacier was either very small and past the topographic threshold or completely melted away). Unit B (core N2: 260-160 cm; core N5: 285-240 cm total sediment depth) is comprised of massive gray clays with very faint laminations, with some moss rich, sandy and gravel layers. Ti concentration, MS, and PC1 scores are variable, and organic matter content is between ~2-5% in core N2 and between ~1.5-4.5% in core N5. Unit B is interpreted as representing a period when the upstream glaciers were smaller than present or absent. The upper unit (A, N2: 160-0 cm) is composed of massive gray clays. Some banding is visible below 122 cm, alternating between a darker gray clay and a lighter gray clay. Unit A has low organic matter content, less than ~2.5% (except for the top 1 cm, LOI is 3.5%), relatively high abundance of Ti, and high MS. PC1 scores reflect minerogenic rich sediment. Unit A is interpreted as a period with glacial meltwater input.

422

423

424

425

426

427

428

429

430

431

432

433

434

435

436

437

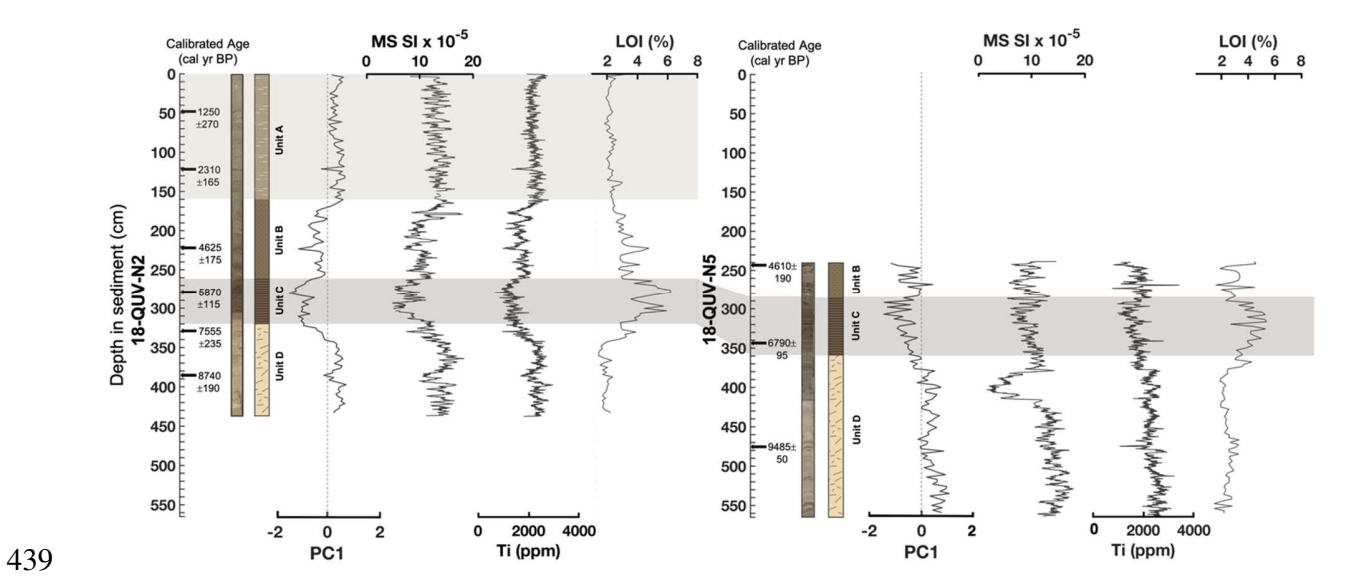


Figure 3. Quvnerit Lake core data. Core images, PC1 scores, MS (10-point moving average), Ti concentration, and LOI. Cores are subdivided into four units. Unit C records non-glacial conditions in the catchment.

4.3. Alakariqssoq

Core 18-ALA-U1 is subdivided into three units (Fig. 4). Core 18-ALA-N1 was also subdivided into three units that clearly correlate with those in core 18-ALA-U1 (Fig. 4). The lower unit (C, core U1: 135-90 cm; core N1: 135-97 cm) is generally gray in color and consists of mainly faintly laminated silty-clays. In core U1, there is a browner, more organic rich layer between 115-113 cm, a moss rich layer from 109-108 cm, and a sandy layer in between, and at 103-100 cm. In core U1 the sediment becomes sandier below 122 cm with gray sandy-silt and clay laminations. In core N1 there is a moss layer between 123-122 cm, and a browner layer between 128-127 cm. Sandy layers are located at 125 and 114 cm in core N1. MS is very high until ~120 cm in core U1 and variable in core N1. Ti concentrations are relatively high with a general decreasing trend toward unit B above. Organic matter content is relatively low, but with

an increasing trend toward unit B above, and averages ~6% in core U1 and 8% in core N1. PC1 scores reflect primarily minerogenic rich sediment. Unit C is interpreted as representing a period with glacial meltwater input, except for a decrease in meltwater input between ~115-113 cm in core U1 and ~127-128 cm in core N1, which corresponds to ~10.6-10.5 ka BP. We also note that, in general, glacial meltwater input and the glaciated area is interpreted to have been declining through Unit C. Unit B (core U1: 90-32 cm; core N1: 97-24 cm) is composed of massive to faintly laminated brown, organic rich gyttja with some aquatic moss throughout. MS is very low and Ti concentrations are low and generally <1000 ppm. Organic matter content is high (between 8-17.5%, averaging ~14% in core U1 and between 9-20%, averaging 15% in core N1). PC1 scores reflect organic rich sedimentation. We interpret this unit as recording a period with no glacial meltwater input, indicating the glaciers in this catchment were completely melted away. The upper unit (A, core U1: 32-0 cm; core N1: 24-0 cm) is comprised of silty-clays, becoming grayer in color towards the top of the core. MS and Ti concentration are relatively high and Ti generally shows an increasing trend toward the top of the core. Organic matter content is low and decreases toward the top of the core. LOI ranges between 1.5-9% (averaging ~5%) in core U1 and between 3-9% (averaging 6%) in core N1. PC1 scores reflect minerogenic rich sedimentation. Unit A is interpreted as a period with renewed glacier growth and increasing glacial meltwater input toward the core tops.

455

456

457

458

459

460

461

462

463

464

465

466

467

468

469

470

471

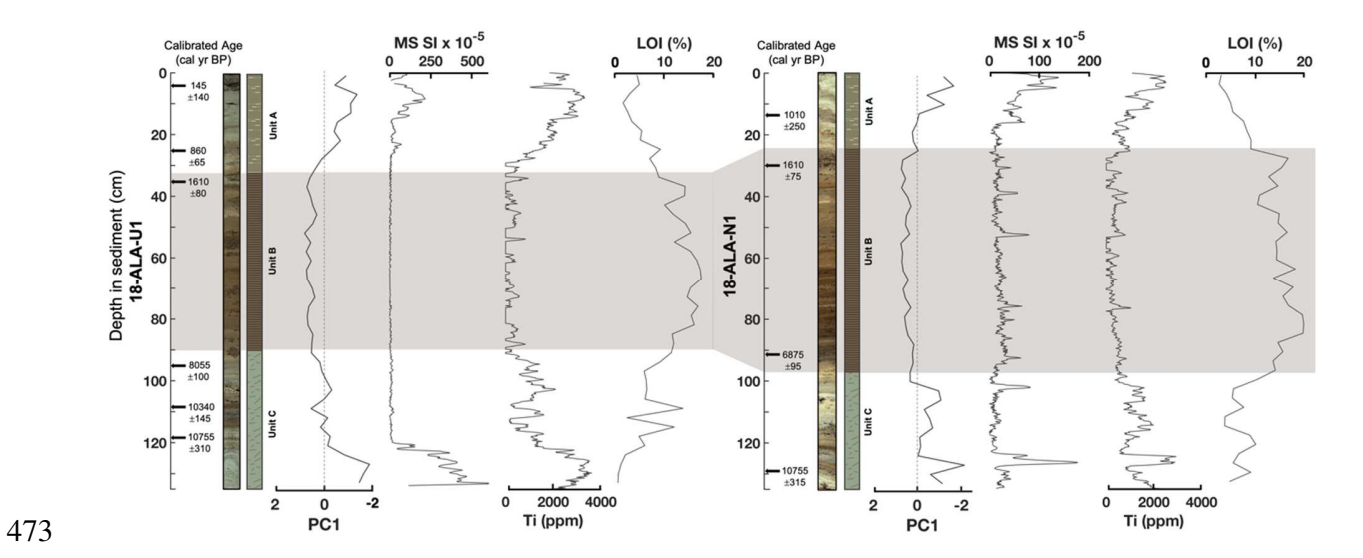


Figure 4. Alakariqssoq lake core data. Core images, PC1 scores, MS, Ti concentration, and LOI. Cores are subdivided into three units. Unit B represents the period in which the local glaciers were interpreted to have completely melted away.

4.4. Uunartoq

18-UUN-U3 is subdivided into three units (Fig. 5). 18-UUN-N2 is subdivided into two units (the upper unit A from core 18-UUN-U3 was not captured in this core, which bypassed the upper ~11 cm of sediment) (Fig. 5). The lower unit (C, core U3: 50-42 cm; core N2: 104-27 cm, total depth below the sediment-water interface) is comprised of dense massive gray silty-clays. MS and Ti concentrations are high, and organic matter content is low (LOI is less than ~5% in core U3 and N2). PC1 scores reflect minerogenic rich sedimentation. Unit C reflects glacial meltwater input to the lake. The transition to Unit B (core U3: 42-12 cm; core N2: 27-11 cm) which is comprised of brown organic rich gyttja is relatively abrupt. Organic matter content increases abruptly at the beginning of the unit and is generally high, peaking ~23% and averaging ~15% in core U3. MS is reduced and Ti concentration is zero or below the detection limit for most of the unit. PC1 scores reflect organic rich sedimentation. The characteristics of

Unit B are indicative of a period when the local glaciers were completely melted away. The sediment of the upper unit (A, core U3: 12-0 cm) becomes increasingly gray in color, and less dense. There is a layer browner in color between 8-6 cm, and band of orange colored sediment at 2 cm. Ti concentration increases and organic matter content decreases to 9% toward the top of the core. PC1 scores reflect the input of minerogenic rich sediments into the lake. Unit A reflects renewed glacier growth and is likely associated with the deposition of the M2 moraines, reflecting the maximum historic extent in the LIA.

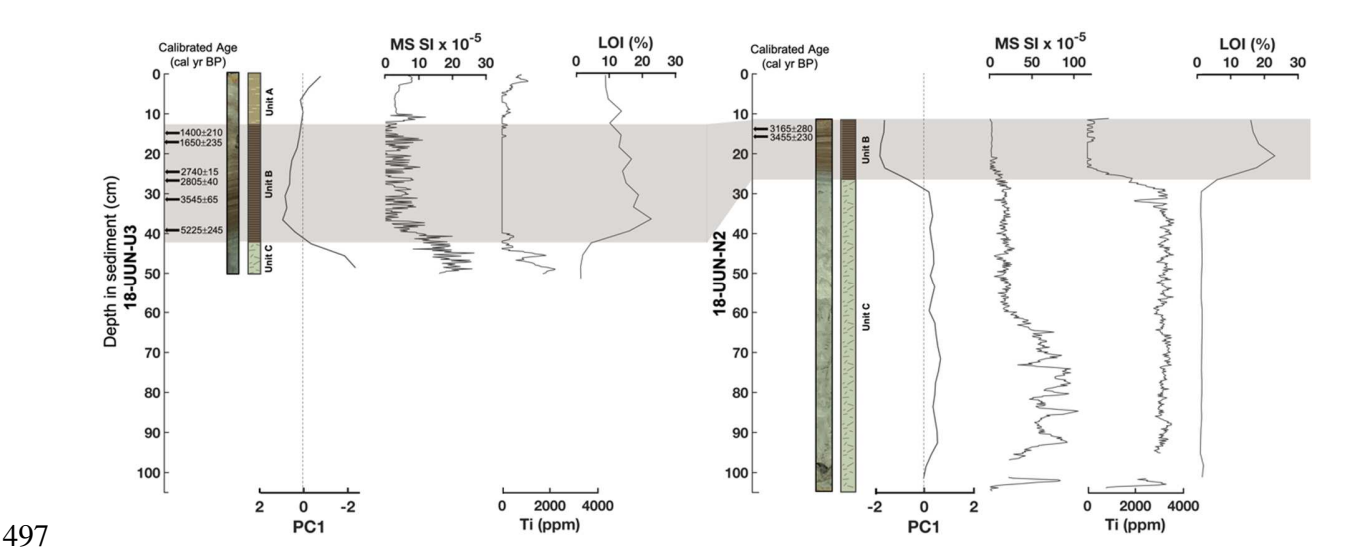


Figure 5. Uunartoq lake core data. Core images, PC1 scores, MS, Ti concentration, and LOI. Cores are subdivided into three units. Unit B represents the period when the local glaciers were interpreted to have completely melted away.

4.5. Equilibrium-line altitudes and summer temperature reconstructions

Here we compare average present (2016-2019) snowlines with estimated glacier ELA minima (assumed to be associated with the LIA) and ELA maxima (assumed to be associated with the onset of the HTM, i.e. the minimum HTM ELA) and report the ablation-season temperature change relative to present required to cause these past ELA shifts (Fig. 6 and Table

3). As described in Methods, we do not account for precipitation change, and consider our LIA and HTM Δ ELA (and resulting inferred temperatures) to be minimum constraints.

We find that the ΔELA (for each lake site we report an average value from multiple glaciers/glacier lobes) and corresponding minimum temperature depression, relative to present during the LIA was –133 meters (or ~0.9°C) at Alakariqssoq; –61 meters (or ~0.4°C) at Uunartoq; and –79 meters (or ~0.5°C) at Quvnerit. We find the ΔELA and minimum HTM temperature rise, relative to present, was +180 meters (or 1.2°C) at Alakariqssoq; +129 meters (or 0.9°C) at Uunartoq; and +180-264 meters (or 1.2-1.8°C) at Quvnerit (with the range at Quvnerit depending upon whether the larger glacier melted beyond the lake's catchment or instead melted away completely). Based on its relatively low elevation, small size (relative to other outlying GICs in Greenland), and southern location, the larger glacier within Quvnerit's catchment most likely melted away completely during the local HTM (e.g., Larsen et al., 2019). Thus, we suggest the larger ΔELA/higher temperature estimate is more representative of minimum HTM summer temperatures in southern Greenland. For reference, present average (1987-2017) summer (JJA) temperature at Qaqortoq (60.72°N, 46.05°W, station no. DMI 04272) is ~7.3°C (Vinther et al., 2006). Preindustrial (1870-1900) average summer (JJA) temperature at Qaqortoq was ~6.5°C (Vinther et al., 2006).

Table 3. Detailed results of geospatial analyses from Quvnerit (QUV), Alakariqssoq (ALA), and
 Uunartoq (UUN) lake sites.

Glacier ID	ELA based on present extent (m a.s.l.)	Average present snowline elevation $\pm 1\sigma$ (m a.s.l.)	# of snowlines digitized	LIA ELA (m a.s.l.)	LIA ΔELA (m)	Minimum LIA ΔT relative to present (°C)	Highest present ice elevation (m a.s.l.)	Critical ΔELA (m)	Minimum HTM ΔT relative to present (°C)
ALA 1	1288	1272±45	6	1015	-257	-1.75	1449	+177	+1.20
ALA 2	1084	1110±26	7	1015	-95	-0.65	1273	+163	+1.11
ALA 3	1128	1163±21	7	1015	-148	-1.01	1322	+159	+1.10

ALA 4	1044	1047±27	7	1015	-32	-0.22	1270	+223	+1.52
UUN 1	990	1048±13	6	1007	-41	-0.28	1116	+68	+0.46
UUN 2	951	1012±16	8	1007	-5	-0.03	1152	+140	+0.95
UUN 3	1147	1152±11	9	1007	-145	-0.99	1369	+217	+1.48
UUN 4	1043	1060±26	18	1007	-53	-0.36	1149	+89	+0.61
*QUV 1	805	854±59	18	767	-87	-0.59	1050/1118	+196/264	+1.33/1.80
QUV 2	712	759±7	5	689	-70	-0.48	923	+164	+1.12

* Two HTM estimates are given for the Quvnerit 1 glacier, see text for details.

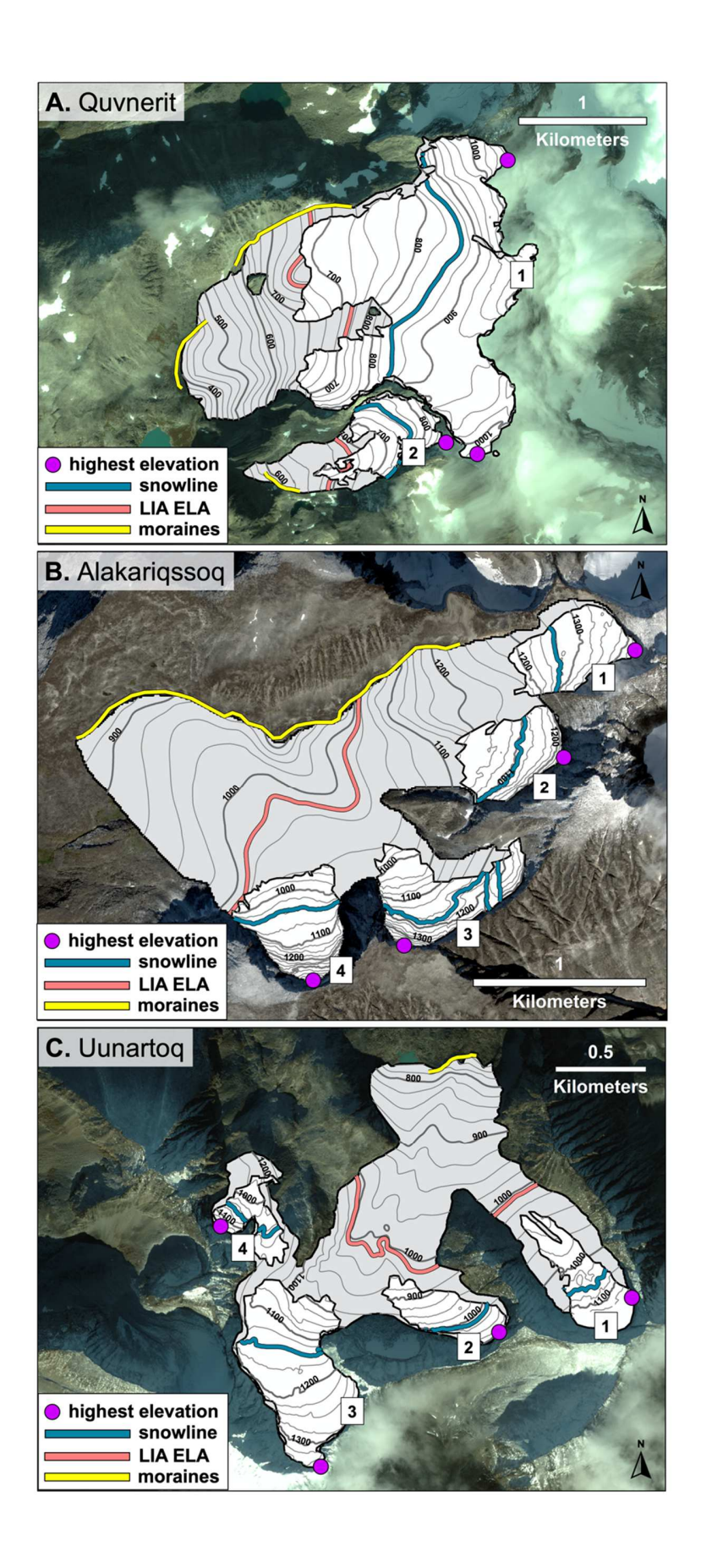


Figure 6. Estimated HTM and LIA ELAs and paleoglacier reconstructions: Quvnerit (**A**), Alakariqssoq (**B**), and Uunartoq lake (**C**). White polygons show extant glacier extents and gray polygons show the modeled LIA paleoglacier extents. The locations of the highest elevation on each extant glacier (used to estimate minimum HTM ELAs) are shown in purple dots. Modeled LIA ELAs are shown as pink lines, modern snowlines as blue lines, and moraines used to reconstruct maximum historic glacier extent are in yellow lines. Thick gray lines show 100 m contours and thin gray lines show 25 m contours. Glacier numbers (in boxes) correspond with Table 3 (2012-2016 late summer Worldview-2 imagery copyright 2019 Digital Globe, Inc.).

5. Discussion

5.1. Holocene climate of southern Greenland and Greenland-wide patterns of GIC variability

Here we summarize the Holocene climate of southern Greenland inferred from our local GIC reconstructions. We also compare our results with other existing paleoclimate records from the region. Glacial lakes Quvnerit and Alakariqssoq formed before ~9.5 ka BP and ~10.75 ka BP respectively, following the early and rapid deglaciation of this region by the GrIS (Carlson et al., 2008). Prior work indicates that the southern GrIS had retreated from the outer coast by ~14.1 to within its near-present margins beginning 11.1 to 10.6 ka BP (Andresen et al., 2004; Björck et al., 2002; Carlson et al., 2014). Thus, we infer that the minerogenic-rich sediment at the beginning of these records is derived from local glaciers, not the GrIS. The Quvnerit and Alakariqssoq lake records show evidence of local glacier meltwater input from the onset of lacustrine sedimentation until ~7.1 and 7.3 ka BP, respectively (Fig. 3, 4, 7B & C). Accordingly, this suggests that South Greenland remained relatively cool in the early Holocene which allowed for GIC presence in the lake catchments. However, the overall decline in major element

abundance, shown in the Ti concentrations from these two records (Fig. 3 & 4), also suggest an overall decline in glacier size, and thus subdued, gradual warming through the early Holocene. In addition, our data suggest that this gradual warming may have been overprinted by significant variability in glacier size at both sites, indicating several glacier expansions, and by inference, early Holocene cooling episodes between ~10.5-8 ka BP (Fig. 7B & C).

553

554

555

556

557

558

559

560

561

562

563

564

565

566

567

568

569

570

571

572

573

574

575

Combined, our sediment records and paleoglacier reconstructions suggest that ablation season temperatures in South Greenland did not exceed 1.2°C warmer than present for a sustained period at Alakarigssoq and Quvnerit in the early Holocene. Summer temperatures exceeding that value would eliminate local glaciers from the lake catchments, thus causing organic sedimentation at these sites. Our early Holocene climate inferences support several review studies that synthesized proxy climate data from the Arctic and suggested, based upon sparse data from the region, that southern Greenland and the Labrador Sea region experienced a relatively cool early Holocene and a delayed thermal maximum (e.g., Kaufman et al., 2004; Kaplan and Wolfe, 2006; Briner et al., 2016). That previous work attributed this pattern to the region's proximity to the diminishing Laurentide Ice Sheet (LIS), which lingered well after peak summer insolation, until ~6.8 ka BP (Kaufman et al., 2004). The waning LIS is thought to have had profound effects on the North Atlantic region during the early Holocene, in part, through episodic freshwater discharge events, and influence on atmospheric circulation and ocean currents and dynamics, including the strength of the North Atlantic subpolar gyre (Kaufman et al., 2004; Kaplan and Wolfe, 2006; Renssen et al., 2007; Briner et al., 2016). In addition to the 8.2 ka BP cold event (which is associated with the catastrophic drainage of ice-dammed glacial lakes in the Hudson Bay area; Hoffman et al., 2012), detrital carbonate peaks from a Labrador shelf marine core record suggests several other abrupt freshwater release events between 11.57.8 ka BP, with the freshwater forcing most marked and sustained between 9.7-7.8 ka BP (Jennings et al., 2015) (Fig. 7I). Early Holocene cold events have also been suggested in other terrestrial records from South Greenland. Although proxy data at Lake Igaliku (Fig. 1) suggests early warmth, the record also indicates an unstable, cold, and windy climate event from 8.6-8.1 ka BP (Massa et al., 2012), and at Lake N14 (Fig. 1 & 7D) a cold and dry period is inferred between 8.4-8.0 ka BP (Andresen et al. 2004).

576

577

578

579

580

581

582

583

584

585

586

587

588

589

590

591

592

593

594

595

596

597

598

At ~7.1 and ~7.3 ka BP, the Quvnerit and Alakarigssoq lake records show a nearly synchronous (within chronological error) disappearance of the local glaciers in their catchments (i.e. shift to organic sedimentation) (Fig. 7B & C). The glaciers within Uunartoq's catchment had also disappeared prior to ~5.2 ka BP (Fig. 7A). However, because we cannot determine the timing of events prior to this date, nor when these glaciers first melted away, we base our early and middle Holocene climate interpretations on the Quvnerit and Alakariqssoq records. Our ΔELA estimates suggest that summer temperatures in southern Greenland exceeded present-day values by at least 1.2-1.8°C in the middle Holocene, by ~7.3-7.1 ka BP. In addition, the concurrent timing of glacier disappearance may indicate that the rate of summer temperature change was relatively fast (e.g. Anderson et al., 2019). Our results indicate that the warmest part of the Holocene at our study sites occurred during the mid-Holocene, between ~7.1-5.5 ka BP, lagging peak summer insolation by several millennia. However, because of the nature of our temperature proxy (i.e. we cannot constrain temperature change beyond the critical ELA), we cannot place a bound on the magnitude of maximum warmth during this period, nor evaluate whether or not the magnitude of mid-Holocene HTM warmth in South Greenland was less than in other regions in Greenland. The general timing of this shift (~7 ka BP) is in good agreement with several other paleoclimate studies from the region. Qipisarqo Lake pollen data show a rapid increase in July surface air temperature at 7.5-7 ka BP (Fig. 7F; Fréchette and Vernal, 2009), and biogenic silica and organic matter abundance suggest a relatively cool climate from the start of the record (at ~9.5 ka BP) up to 8 ka BP, and warmer and more stable conditions between 6-3 ka BP (Fig. 7G; Kaplan et al., 2002). Similarly, further south, percent biogenic silica data from Lake N14 suggest relatively warm and stable conditions between 8-5 ka BP, with cooler and less stable conditions before and after (Fig. 7D; Andresen et al., 2004). In addition, a threshold lake record located near the southern GrIS's present margin shows that following deglaciation, a portion of the southern GrIS retreated to its present-day extent by ~10.6 ka BP, but remained nearby until ~6.9 cal BP, at which time it retreated beyond the lake's watershed (Larsen et al., 2011).

Across Greenland, the timing of local GIC disappearance (or reduction in extent), in response to warmer than present conditions, appears to be associated with latitude (Fig. 8). In general, GICs in northern Greenland first became smaller than today or absent earlier in the Holocene than those in the south. GICs above 70°N (Fig. 8H, I, J, K & L) first became smaller or disappeared between ~10.2-9.4 ka BP. GICs ~65°N (Fig. 8D, E, F, & G) first became smaller or disappeared between ~9.5-7.9 ka BP. And, GICs below 61°N (Fig. 8A & C; i.e. those in this study) first disappeared between ~7.3-7.1 ka BP. This pattern is consistent with the north-to-south trend in the timing of HTM warmth tentatively observed in the review of temperature-sensitive proxy records by Briner et al. (2016) and supports the notion that climatic responses across Greenland to insolation and other forcings through the Holocene were complex.

We find renewed local glacier growth in Alakariqssoq and Uunartoq's catchments at ~1.3 and ~1.2 ka BP, respectively (Fig. 7A & B). Quvnerit lake, which today sits in a wetter area and hosts the largest glacier, shows evidence for persistent glacial input the earliest of the three sites,

beginning at ~3.1 ka BP (Fig. 7C). The renewed presence of local glaciers occurred during the late Holocene as northern hemisphere summer insolation declined and climate cooled. The Quvnerit lake record provides the best estimate of the onset of regional Neoglaciation, ~3.1 ka BP, and this timing corresponds with other evidence for regional cooling. Sediments of lake N14 suggest the first signs of a transition from Holocene optimum conditions at 4.7 ka BP, and cooler and drier conditions from 3.7 ka BP (Fig. 7D; Andresen et al., 2004). The Lake Igaliku record shows a transition to moist and cooler conditions at ~4.8 ka BP, with more significant cooling after ~3 ka BP (Massa et al., 2012). At Qipisarqo Lake, a decrease in biogenic silica indicates marked cooling after ~3 ka BP (Fig. 7G; Kaplan et al., 2002).

The late Holocene timing of glacier regrowth in the Quvnerit, Alakariqssoq, and Uunartoq catchments is in good agreement with several other glacial records from Greenland (Fig. 8) and the North Atlantic region suggesting a response to common forcing mechanisms (Bakke et al., 2010; Solomina et al., 2015; Schweinberg et al., 2017; van der Bilt et al., 2019). In southwest Greenland, renewed ice growth is recorded in the Badesø and Langesø lake catchments at ~3.6-3.5 ka BP (Fig. 8 D1 & D2; Larsen et al., 2017), and in the southeast at Kulusuk lake, renewed ice growth is recorded at ~4.1 ka BP followed by several centennial-scale glacier advances between ~4.1-1.3 ka BP (Fig. 8E; Balascio et al., 2015). In west Greenland, snowline lowering, and an episode of glacier expansion is recorded at ~3.7 ka BP, which the study notes, coincides with colder ocean conditions in Disko Bugt and in the North Atlantic (Fig. 8 H1; Schweinberg et al., 2017). In two other lake catchments in west Greenland, GIC regrowth is recorded ~4.3 ka BP with significant glacier expansion phases at ~3.7 and 2.8 ka BP (Fig. 8 H2 & H3; Schweinberg et al., 2019). Later in the Holocene, in southeast Greenland, glaciers reformed in the Ymer lake catchment at ~1.2 ka BP (Fig. 8F; van der Bilt et al., 2018), and a

glacier advance is recorded at the Kulusuk lake catchment at ~1.3 ka BP (Fig. 8E; Balascio et al., 2015). In the southwest, renewed local glacier growth is recorded at ~1.6 ka BP at lake IS21 along with an advance between ~1.6-1.4 ka BP (Fig. 8 D3; Larsen et al., 2017), and at nearby Crash lake, an interval of glacier expansion is recorded at ~1.2 ka BP (Fig. 8G; Schweinberg et al., 2018). Similarly, in west Greenland, a glacier advance following snow-line lowering is recorded at Sikuiui lake ~1.4 ka BP (Fig. 8 H1; Shweinsberg et al., 2017). A recent review which combines proxy evidence of glacier and sea-ice change with a climate model experiment suggests that Arctic Atlantic climate shifted toward a colder mean state around 1.3-1.0 ka BP, and that unforced sea-ice feedbacks best explain this climate deterioration triggering pre-LIA glacier expansion across the North Atlantic Arctic (van der Bilt et al., 2019). Other studies also note these synchronous, late Holocene glacier responses in Greenland and the North Atlantic (e.g., Bakke et al., 2010; Balascio et al., 2015; Larsen et al., 2017) and suggest a connection between GIC change and shifts in ocean/atmosphere circulation, sea-ice feedbacks, and/or solar forcing and volcanic perturbations (Miller et al., 2012; Geirsdóttir et al., 2013; Solomina et al., 2015; Kobashi et al., 2017; Schweinberg et al., 2017; 2018; 2019).

The combined effects of local climate, the rate of summer temperature change, topography, and glacier hypsometry may have also influenced the timing of local glacier regrowth across Greenland in the late Holocene (Fig. 8). Larsen et al. (2017) highlighted this topographic sensitivity and showed that for three glaciers in close proximity, the glacier situated at the highest elevation regrew first as summer temperatures cooled and ELA moved down to intersect the local landscape. A recent study on Icelandic GICs suggests that the rate of summer temperature change was a central control on regional glacier regrowth (Anderson et al., 2019). With overall slow rates of summer cooling, such as those from the middle to late Holocene,

modeling results show little spatial correlation and a wide range in the timing of glacier inception within a region (Anderson et al., 2019). Thus, synchronous timing of GIC regrowth or advance may possibly cluster around times with increased cooling rates (e.g., McKay et al., 2018). Local climatic factors may also be important determinants of site-to-site variations in glacier history. Within our study, the most southern and lowest-elevation glaciers (within Quvnerit's watershed) regrew first, with persistent glacial input after ~3.1 ka BP. We suggest that the earlier regrowth of this glacier was in part due to the area's very high precipitation rates, which today are ~2-4 times that of our other two study sites according to near-by weather stations (Cappelen et al., 2001) and an ERA-Interim reanalysis surface mass balance (SMB) model (Fettweis, 2007), and thus can support lower ELAs. Currently Quvnerit's glaciers have snowlines/ELAs that are ~300-400 m lower in elevation than the glaciers at Alakariqssoq and Uunartoq. The local glaciers within Alakariqssoq's and Uunartoq's watersheds—which are close geographically, at similar elevations, and similar in size—show a synchronous timing of regrowth between ~1.3-1.2 ka BP.

We infer increasing glacial meltwater input reflecting growth to maximum late Holocene glacier extents during the LIA (~0.2-0.1 ka BP) at all three study sites. Based on the maximum historical moraine limits, our paleoglacier results indicate a LIA temperature depression of at least 0.4-0.9°C. Similarly, during this second, colder portion of the LIA, Kaplan et al. (2002) reported that the ice sheet outlet glacier, Nordre Qipisarqo Bræ, advanced into the catchment of Qipisarqo Lake for the first time during their ~9.5 ka record, and Massa et al. (2012) found minimum pollen accumulation rates indicating cold conditions (between ~1500 and 1920 AD) (~0.45-0.03 ka BP).

Overall, given the strong correspondence between our results and independent paleoclimate interpretations in the region (Fig. 7), we suggest that southern Greenland's GICs

responded both sensitively and quickly, on a scale of decades to centuries, to climate changes through the Holocene. Consequently, we expect that GICs in the region will rapidly diminish due to anthropogenic warming in the coming decades. Based on our modeled ELAs, which assumes no change in precipitation, we find that a rise in summer temperatures of ~0.5-1.8°C above present would render all our studied glaciers ablation zones, which would lead to their swift disappearance, with the smaller glaciers likely melting away first.

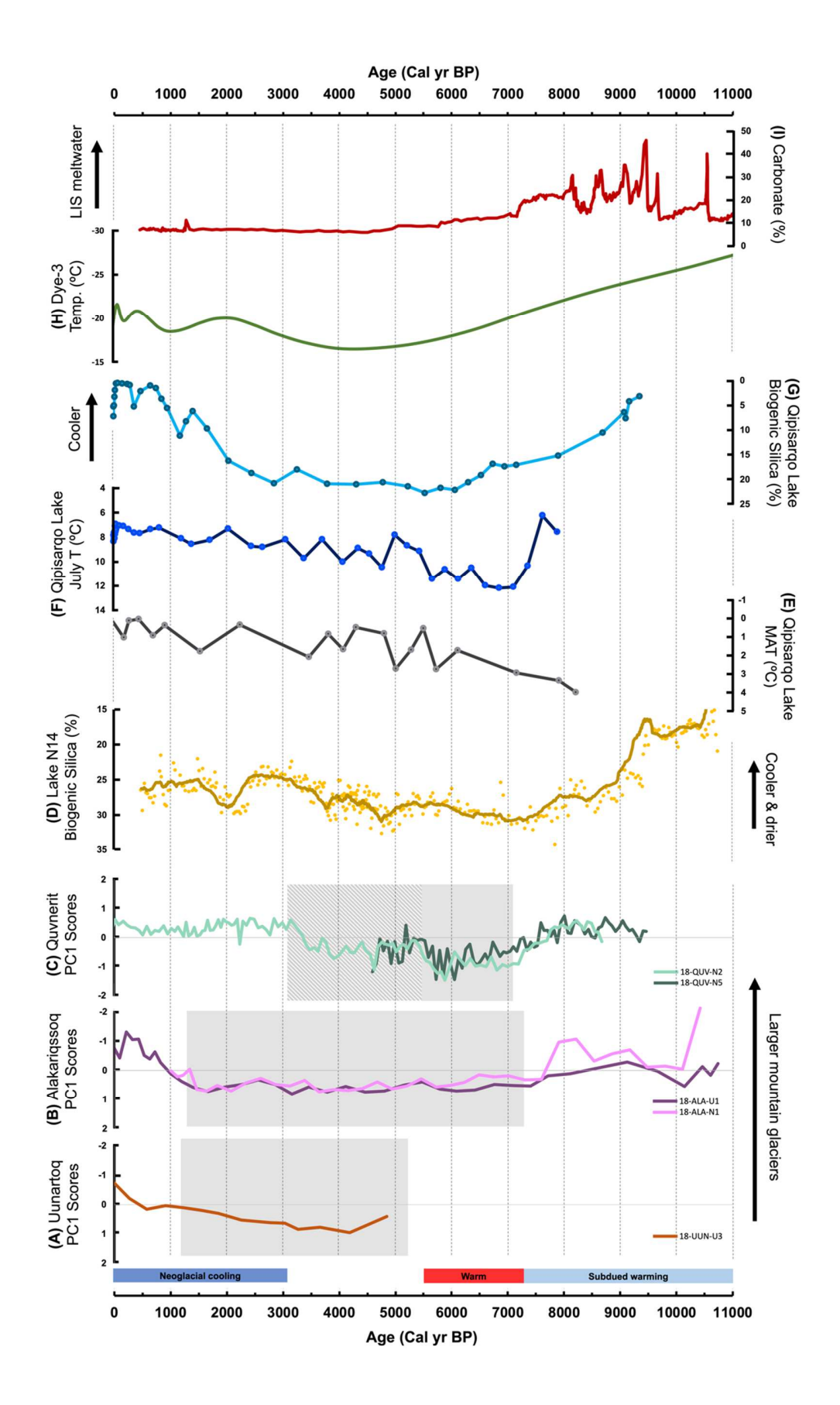


Figure 7. Summary of southern Greenland climate reconstructions and local glacier fluctuations. Bottom colored bars summarize the major inferences made by this study. **A-C.** PC1 scores for Uunartoq, Alakariqssoq, and Quvnerit showing fluctuations in glacier size and relative summer air temperature. Solid gray bars show periods when the local glaciers at each site are interpreted to have melted away completely (or in the case of Quvnerit's larger glacier, at least retreated outside the lake's watershed). The striped gray bar shows periods when local glaciers are interpreted to have been smaller than present or absent. **D.** Percent biogenic silica from Lake N14. The yellow line is a 25-point moving average (Andresen et al., 2004). **E-G.** Qipisarqo Lake proxy records. Mean annual air temperature (MAT) inferred from δ^{18} O of chironomid head capsules (Wooller et al., 2004), July surface air temperature (T) inferred from pollen assemblages (Fréchette and Vernal, 2009), and percent biogenic silica (Kaplan et al., 2002). **H.** Dye-3 borehole temperature (Dahl-Jensen et al., 1998). **I.** Detrital carbonate abundance indicating freshwater input from the LIS into the Labrador Sea (Jennings et al., 2015).

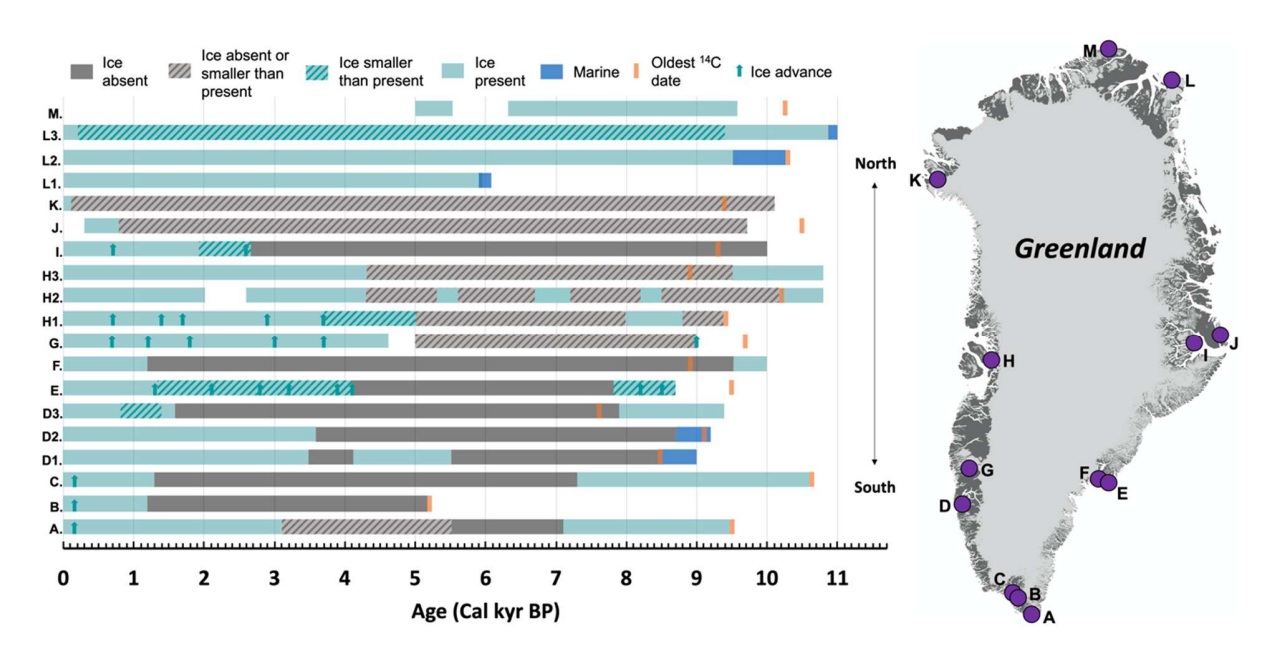


Figure 8. Summary of Holocene local glacier and ice cap reconstructions in Greenland. Study including author & year, and lake and/or glacier name as follows: A. This study, Quvnerit; B. This study, Uunartoq; C. This study, Alakariqssoq; D. Larsen et al., 2017, D1. Badesø, D2. Langesø, D3. IS21; E. Balascio et al., 2015, Kulusuk; F. van der Bilt et al., 2018, Ymer; G. Schweinsberg et al., 2018, Crash; H. Schweinsberg et al., 2017; 2019, H1. Sikuiui, H2. Saqqap Tasersua, H3. Pauiaivik; I. Levy et al., 2014, Bregne/Two Move; J. Lowell et al., 2013; Istorvet/Bone; K. Axford et al., 2019, Deltasø/North Ice Cap; L. Larsen et al., 2019, L1. Ice cap 1/T4, **L2.** Ice cap 2/T6 & T2, **L3.** Flade Isblink/T3 & T8; **M.** Möller et al., 2010, Sifs.

6. Conclusions

In this study, we present three continuous records of local glacier fluctuations in the Kujalleq region, South Greenland, spanning the past ~10.75 ka. We also use geospatial tools to provide estimates of glacier ELA change during the warmest and coldest parts of the Holocene, giving a magnitude of minimum ablation-season temperature change relative to present. From the onset of the lake sediment records until ~7.3 and ~7.1 ka BP, summer temperatures permitted the presence of local glaciers in the Alakariqssoq and Quvnerit lake catchments. Changes in lake sediment composition also record gradually shrinking glacier size and thus suggest gradual, subdued warming throughout the early Holocene, overprinted by shorter-term local glacier advances possibly reflecting multiple regional cooling episodes between ~10.5-8 ka BP. At ~7.1 and ~7.3 ka BP, the Quvnerit and Alakariqssoq records show a nearly synchronous shift to organic, non-glacial sedimentation recording the disappearance of local glaciers, while Uunartoq's glaciers disappeared prior to ~5.2 ka BP. We infer from reconstructed ΔELAs that summer temperatures were at least 1.2-1.8°C warmer than present by ~7.3-7.1 ka BP. Our records are in good agreement with other studies which suggest that southern Greenland and the

Labrador Sea region experienced a delayed thermal maximum (relative to summer insolation forcing and to climate at sites farther north). GIC records from across Greenland show a corresponding latitudinal trend, with local glaciers in northern Greenland becoming smaller than their current sizes or disappearing earlier in the Holocene than those in the south. We document the long-term reappearance of local glaciers at ~3.1, ~1.3 and ~1.2 ka BP in South Greenland, reflecting a broad Arctic pattern of cooling summer air temperatures in the late Holocene. The timing of late Holocene glacier regrowth in the three lake catchments is in agreement with other GIC reconstructions from Greenland and the North Atlantic region. Finally, during the second and more severe portion of the LIA, ~0.2-0.1 ka BP, maximum historical moraine extents and modeled LIA ELAs at each site indicate that summer temperatures cooled by at least 0.4-0.9°C. Given the fast response and high sensitivity of GICs to changing summer temperatures throughout the Holocene, we expect that ongoing anthropogenic warming will cause southern Greenland's GICs to lose their accumulation zones and ultimately disappear within this century.

Acknowledgements

This research was supported by the U.S. National Science Foundation's Office of Polar Programs (CAREER Award 1454734) and Geography and Spatial Sciences Program (DDRI Award 1812764), the National Geographic Society (grant 9694-15), and a Northwestern University undergraduate research grant. We thank the people and government of Greenland for site access (survey license VU-00130 and export permit 171/2018); M. Chipman, P. Puleo, and A. Hartz for assistance with field work; T. Axford for designing and building field equipment; Polar Field Services and J. Simund for logistical support; Air Greenland for helicopter support; the U.S. Air National Guard for transport to and from Greenland; R. Steigleder, A. Hansen, and G. Schellinger for lab assistance; Woods Hole Oceanographic Institution - National Ocean Sciences Accelerator Mass Spectrometry facility for radiocarbon analysis; the United States Geological Survey (USGS), and Google Earth Engine for satellite imagery; and the Polar Geospatial Center (PGC) for satellite imagery and digital elevation models (DEMs). DEMs provided by the Polar Geospatial Center under NSF-OPP awards 1043681, 1559691, and 1542736. Geospatial support for this work provided by the Polar Geospatial Center under NSF-OPP awards 1043681 and 1559691. Finally, we thank Willem G.M. van der Bilt and one anonymous reviewer for improving this manuscript.

767 768

References

- Alley, R.B., 2003. Comment on "When Earth's Freezer Door is Left Ajar". EOS, Transactions American Geophysical Union 84, 315. doi:10.1029/2003EO330004
- Anderson, L.S., Geirsdóttir, Á., Flowers, G.E., Wickert, A.D., Aðalgeirsdóttir, G., Thorsteinsson,
 T., 2019. Controls on the lifespans of Icelandic ice caps. Earth and Planetary Science Letters
- 774 527, 115780. doi:10.1016/j.epsl.2019.115780
- Andresen, C.S., Björck, S., Bennike, O., Bond, G., 2004. Holocene climate changes in southern Greenland: evidence from lake sediments. Journal of Quaternary Science 19, 783–795.
- 777 doi:10.1002/jqs.886
- Axford, Y., Lasher, G., Kelly, M., Osterberg, E., Landis, J., Schellinger, G., Pfeiffer, A.,
- 779 Thompson, E., Francis, D., 2019. Holocene temperature history of northwest Greenland –
- With new ice cap constraints and chironomid assemblages from Deltasø. Quaternary Science
- 781 Reviews 215, 160–172. doi:10.1016/j.quascirev.2019.05.011
- Bakke, J., Dahl, S.O., Paasche, Ø., Simonsen, J.R., Kvisvik, B., Bakke, K., Nesje, A., 2010. A
- complete record of Holocene glacier variability at Austre Okstindbreen, northern Norway: an
- integrated approach. Quaternary Science Reviews 29, 1246–1262.
- 785 doi:10.1016/j.quascirev.2010.02.012
- Balascio, N.L., Dandrea, W.J., Bradley, R.S., 2015. Glacier response to North Atlantic climate variability during the Holocene. Climate of the Past Discussions 11, 2009–2036.
- 788 doi:10.5194/cpd-11-2009-2015
- 789 Benn, D.I., Lehmkuhl, F., 2000. Mass balance and equilibrium-line altitudes of glaciers in high-
- mountain environments. Quaternary International 65-66, 15–29. doi:10.1016/s1040-
- 791 6182(99)00034-8
- Benn, D.I., Hulton, N.R., 2010. An ExcelTM spreadsheet program for reconstructing the surface
- profile of former mountain glaciers and ice caps. Computers & Geosciences 36, 605–610.
- 794 doi:10.1016/j.cageo.2009.09.016
- Bintanja, R., Selten, F.M., 2014. Future increases in Arctic precipitation linked to local evaporation and sea-ice retreat. Nature 509, 479–482. doi:10.1038/nature13259
- 797 Björck, S., Bennike, O., Rosén, P., Andresen, C.S., Bohncke, S., Kaas, E., Conley, D., 2002.
- Anomalously mild Younger Dryas summer conditions in southern Greenland. Geology 30,
- 799 427. doi:10.1130/0091-7613(2002)030<0427:amydsc>2.0.co;2
- Bjørk, A.A., Aagaard, S., Lütt, A., Khan, S.A., Box, J.E., Kjeldsen, K.K., Larsen, N.K.,
- Korsgaard, N.J., Cappelen, J., Colgan, W.T., Machguth, H., Andresen, C.S., Peings, Y., Kjær,
- K.H., 2017. Changes in Greenland's peripheral glaciers linked to the North Atlantic
- 803 Oscillation. Nature Climate Change 8, 48–52. doi:10.1038/s41558-017-0029-1
- Bjørk, A.A., Kjær, K.H., Korsgaard, N.J., Khan, S.A., Kjeldsen, K.K., Andresen, C.S., Box, J.E.,
- Larsen, N.K., Funder, S., 2012. An aerial view of 80 years of climate-related glacier
- fluctuations in southeast Greenland. Nature Geoscience 5, 427–432. doi:10.1038/ngeo1481

- Blaauw, M., Christen, J.A., 2011. Flexible paleoclimate age-depth models using an autoregressive gamma process. Bayesian Analysis 6, 457–474. doi:10.1214/11-ba618
- Braithwaite, R.J. and Müller, F., 1980. On the parameterization of glacier equilibrium line
- altitude. World glacier inventory. Proc. workshop, Riederalp, Switzerland, 17-22 September
- 811 1978, International Association of Hydrological Sciences, Washington DC; IAHS-AISH
- Publication 126, 263-271.
- Briner, J.P., Mckay, N.P., Axford, Y., Bennike, O., Bradley, R.S., Vernal, A.D., Fisher, D.,
- Francus, P., Fréchette, B., Gajewski, K., Jennings, A., Kaufman, D.S., Miller, G., Rouston,
- 815 C., Wagner, B., 2016. Holocene climate change in Arctic Canada and Greenland. Quaternary
- Science Reviews 147, 340–364. doi:10.1016/j.quascirev.2016.02.010
- 817 Cappelen, J., Jørgensen, B.V., Laursen, E.V., Stannius, L.S. and Thomsen, R.S., 2001. The
- observed climate of Greenland, 1958–99—with climatological standard normals, 1961–90.
- Danish Meteorological Institute. Technical Report 00-18.
- 820 Carlson, A.E., Stoner, J.S., Donnelly, J.P., Hillaire-Marcel, C., 2008. Response of the southern
- Greenland Ice Sheet during the last two deglaciations. Geology 36, 359.
- 822 doi:10.1130/g24519a.1
- 823 Carlson, A.E., Winsor, K., Ullman, D.J., Brook, E.J., Rood, D.H., Axford, Y., Legrande, A.N.,
- Anslow, F.S., Sinclair, G., 2014. Earliest Holocene south Greenland ice sheet retreat within
- its late Holocene extent. Geophysical Research Letters 41, 5514–5521.
- 826 doi:10.1002/2014gl060800
- Dahl, S.O., Nesje, A., 1992. Paleoclimatic implications based on equilibrium-line altitude
- depressions of reconstructed Younger Dryas and Holocene cirque glaciers in inner Nordfjord,
- western Norway. Palaeogeography, Palaeoclimatology, Palaeoecology 94, 87–97.
- 830 doi:10.1016/0031-0182(92)90114-k
- Dahl, S.O., Bakke, J., Lie, Ø., Nesje, A., 2003. Reconstruction of former glacier equilibrium-line
- altitudes based on proglacial sites: an evaluation of approaches and selection of sites.
- 833 Quaternary Science Reviews 22, 275–287. doi:10.1016/s0277-3791(02)00135-x
- Dahl-Jensen, D., 1998. Past Temperatures Directly from the Greenland Ice Sheet. Science 282,
- 835 268–271. doi:10.1126/science.282.5387.268
- Fausto, R.S., Ahlstrøm, A.P., As, D.V., Bøggild, C.E., Johnsen, S.J., 2009. A new present-day
- temperature parameterization for Greenland. Journal of Glaciology 55, 95–105.
- 838 doi:10.3189/002214309788608985
- Fettweis, X., 2007. Reconstruction of the 1979–2006 Greenland ice sheet surface mass balance
- using the regional climate model MAR. The Cryosphere Discussions 1, 123–168.
- 841 doi:10.5194/tcd-1-123-2007
- Fréchette, B., Vernal, A.D., 2009. Relationship between Holocene climate variations over
- southern Greenland and eastern Baffin Island and synoptic circulation pattern. Climate of the
- Past Discussions 5, 879–910. doi:10.5194/cpd-5-879-2009
- Gajewski, K., 2015. Quantitative reconstruction of Holocene temperatures across the Canadian
- Arctic and Greenland. Global and Planetary Change 128, 14–23.
- 847 doi:10.1016/j.gloplacha.2015.02.003

- 648 Geirsdóttir, Á., Miller, G.H., Larsen, D.J., Ólafsdóttir, S., 2013. Abrupt Holocene climate
- transitions in the northern North Atlantic region recorded by synchronized lacustrine records
- in Iceland. Quaternary Science Reviews 70, 48–62. doi:10.1016/j.quascirev.2013.03.010
- Gross, G., Kerschner, H. and Patzelt, G., 1976. Methodische Untersuchungen über die
- Schneegrenze in alpinen Gletschergebieten. Zeitschrift für Gletscherkd. und Glazialgeol 12,
- 853 223–251.
- Heiri, O., Lotter, A.F. and Lemcke, G., 2001. Loss on ignition as a method for estimating organic
- and carbonate content in sediments: reproducibility and comparability of results. Journal of
- paleolimnology, 25(1), pp.101-110. doi:10.1023/A:1008119611481
- Hoffman, J.S., Carlson, A.E., Winsor, K., Klinkhammer, G.P., LeGrande, A.N., Andrews, J.T.,
- Strasser, J.C., 2012. Linking the 8.2 ka event and its freshwater forcing in the Labrador Sea.
- Geophys. Res. Lett. 39, L18703. http://dx.doi.org/10.1029/2012GL053047.
- Jansson, P., Rosqvist, G., Schneider, T., 2005. Glacier fluctuations, suspended sediment flux and
- glacio-lacustrine sediments. Geografiska Annaler: Series A, Physical Geography 87, 37–50.
- 862 doi:10.1111/j.0435-3676.2005.00243.x
- Jennings, A., Andrews, J., Pearce, C., Wilson, L., Ólfasdótttir, S., 2015. Detrital carbonate peaks
- on the Labrador shelf, a 13–7ka template for freshwater forcing from the Hudson Strait outlet
- of the Laurentide Ice Sheet into the subpolar gyre. Quaternary Science Reviews 107, 62–80.
- 866 doi:10.1016/j.quascirev.2014.10.022
- Kaplan, M.R., Wolfe, A.P., Miller, G.H., 2002. Holocene Environmental Variability in Southern
- Greenland Inferred from Lake Sediments. Quaternary Research 58, 149–159.
- 869 doi:10.1006/qres.2002.2352
- 870 Kaplan, M.R., Wolfe, A.P., 2006. Spatial and temporal variability of Holocene temperature in
- the North Atlantic region. Quaternary Research 65, 223–231.
- 872 doi:10.1016/j.yqres.2005.08.020
- 873 Kaufman, D., 2004. Holocene thermal maximum in the western Arctic (0–180°W). Quaternary
- 874 Science Reviews 23, 529–560. doi:10.1016/j.quascirev.2003.09.007
- Kelly, M.A., Lowell, T.V., 2009. Fluctuations of local glaciers in Greenland during latest
- Pleistocene and Holocene time. Quaternary Science Reviews. 28, 2088-2106.
- 877 doi:10.1016/j.quascirev.2008.12.008.
- Kobashi, T., Menviel, L., Jeltsch-Thömmes, A., Vinther, B.M., Box, J.E., Muscheler, R.,
- Nakaegawa, T., Pfister, P.L., Döring, M., Leuenberger, M., Wanner, H., Ohmura, A., 2017.
- Volcanic influence on centennial to millennial Holocene Greenland temperature change.
- 881 Scientific Reports 7. doi:10.1038/s41598-017-01451-7
- Larsen, N.K., Kjær, K.H., Olsen, J., Funder, S., Kjeldsen, K.K., Nørgaard-Pedersen, N., 2011.
- Restricted impact of Holocene climate variations on the southern Greenland Ice Sheet.
- Quaternary Science Reviews 30, 3171–3180. doi:10.1016/j.quascirev.2011.07.022
- Larsen, N.K., Kjær, K.H., Lecavalier, B., Bjørk, A.A., Colding, S., Huybrechts, P., Jakobsen,
- K.E., Kjeldsen, K.K., Knudsen, K.-L., Odgaard, B.V., Olsen, J., 2015. The response of the
- southern Greenland ice sheet to the Holocene thermal maximum. Geology 43, 291–294.
- 888 doi:10.1130/g36476.1

- Larsen, N.K., Find, J., Kristensen, A., Bjørk, A.A., Kjeldsen, K.K., Odgaard, B.V., Olsen, J.,
- Kjær, K.H., 2016. Holocene ice marginal fluctuations of the Qassimiut lobe in South
- Greenland. Scientific Reports 6. doi:10.1038/srep22362
- Larsen, N.K., Strunk, A., Levy, L.B., Olsen, J., Bjørk, A., Lauridsen, T.L., Jeppesen, E.,
- Davidson, T.A., 2017. Strong altitudinal control on the response of local glaciers to Holocene
- climate change in southwest Greenland. Quaternary Science Reviews 168, 69–78.
- 895 doi:10.1016/j.quascirev.2017.05.008
- Larsen, N.K., Levy, L.B., Strunk, A., Søndergaard, A.S., Olsen, J., Lauridsen, T.L., 2019. Local
- ice caps in Finderup Land, North Greenland, survived the Holocene Thermal Maximum.
- 898 Boreas 48, 551–562. doi:10.1111/bor.12384
- 899 Lasher, G.E., Axford, Y., Mcfarlin, J.M., Kelly, M.A., Osterberg, E.C., Berkelhammer, M.B.,
- 900 2017. Holocene temperatures and isotopes of precipitation in Northwest Greenland recorded
- in lacustrine organic materials. Quaternary Science Reviews 170, 45–55.
- 902 doi:10.1016/j.quascirev.2017.06.016
- 903 Lassen, S.J., Kuijpers, A., Kunzendorf, H., Hoffmann-Wieck, G., Mikkelsen, N., Konradi, P.,
- 904 2004. Late-Holocene Atlantic bottom-water variability in Igaliku Fjord, South Greenland,
- 905 reconstructed from foraminifera faunas. The Holocene 14, 165–171.
- 906 doi:10.1191/0959683604hl699rp
- 907 Lea, J.M., 2018. The Google Earth Engine Digitisation Tool (GEEDiT) and the Margin change
- Quantification Tool (MaQiT) simple tools for the rapid mapping and quantification of
- changing Earth surface margins. Earth Surface Dynamics 6, 551–561. doi:10.5194/esurf-6-
- 910 551-2018
- 911 Lecavalier, B.S., Fisher, D.A., Milne, G.A., Vinther, B.M., Tarasov, L., Huybrechts, P., Lacelle,
- D., Main, B., Zheng, J., Bourgeois, J., Dyke, A.S., 2017. High Arctic Holocene temperature
- 913 record from the Agassiz ice cap and Greenland ice sheet evolution. Proceedings of the
- 914 National Academy of Sciences 114, 5952–5957. doi:10.1073/pnas.1616287114
- 915 Leclercq, P.W., Weidick, A., Paul, F., Bolch, T., Citterio, M., Oerlemans, J., 2012. Brief
- communication: Historical glacier length changes in West Greenland. The Cryosphere
- 917 Discussions 6, 3491–3501. doi:10.5194/tcd-6-3491-2012
- Levy, L.B., Kelly, M.A., Lowell, T.V., Hall, B.L., Hempel, L.A., Honsaker, W.M., Lusas, A.R.,
- Howley, J.A., Axford, Y.L., 2014. Holocene fluctuations of Bregne ice cap, Scoresby Sund,
- east Greenland: a proxy for climate along the Greenland Ice Sheet margin. Quaternary
- 921 Science Reviews 92, 357–368. doi:10.1016/j.quascirev.2013.06.024
- Lowell, T.V., 2000. As climate changes, so do glaciers. Proceedings of the National Academy of
- 923 Sciences 97, 1351–1354. doi:10.1073/pnas.97.4.1351
- Lowell, T.V., Hall, B.L., Kelly, M.A., Bennike, O., Lusas, A.R., Honsaker, W., Smith, C.A.,
- Levy, L.B., Travis, S., Denton, G.H., 2013. Late Holocene expansion of Istorvet ice cap,
- 926 Liverpool Land, east Greenland. Quaternary Science Reviews 63, 128–140.
- 927 doi:10.1016/j.quascirev.2012.11.012
- 928 Massa, C., Perren, B.B., Gauthier, É., Bichet, V., Petit, C., Richard, H., 2012. A multiproxy
- evaluation of Holocene environmental change from Lake Igaliku, South Greenland. Journal
- 930 of Paleolimnology 48, 241–258. doi:10.1007/s10933-012-9594-5

- 931 Mcfarlin, J.M., Axford, Y., Osburn, M.R., Kelly, M.A., Osterberg, E.C., Farnsworth, L.B., 2018.
- Pronounced summer warming in northwest Greenland during the Holocene and Last
- 933 Interglacial. Proceedings of the National Academy of Sciences 115, 6357–6362.
- 934 doi:10.1073/pnas.1720420115
- 935 Mckay, N.P., Kaufman, D.S., Routson, C.C., Erb, M.P., Zander, P.D., 2018. The Onset and Rate
- of Holocene Neoglacial Cooling in the Arctic. Geophysical Research Letters 45.
- 937 doi:10.1029/2018gl079773
- 938 Meier, M.F., 1962. Proposed Definitions for Glacier Mass Budget Terms. Journal of Glaciology
- 939 4, 252–263. doi:10.3189/s0022143000027544
- 940 Miller, G.H., Geirsdóttir, Á., Zhong, Y., Larsen, D.J., Otto-Bliesner, B.L., Holland, M.M.,
- Bailey, D.A., Refsnider, K.A., Lehman, S.J., Southon, J.R., Anderson, C., Björnsson, H.,
- Thordarson, T., 2012. Abrupt onset of the Little Ice Age triggered by volcanism and
- sustained by sea-ice/ocean feedbacks. Geophysical Research Letters 39.
- 944 doi:10.1029/2011gl050168
- Möller, P., Larsen, N.K., Kjær, K.H., Funder, S., Schomacker, A., Linge, H., Fabel, D., 2010.
- Early to middle Holocene valley glaciations on northernmost Greenland. Quaternary Science
- 947 Reviews 29, 3379–3398. doi:10.1016/j.quascirev.2010.06.044
- Nesje, A., 1989. Glacier-front variations of outlet glaciers from Jostedalsbreen and climate in the
- Jostedalsbre region of western Norway in the period 1901-80. Norsk Geografisk Tidsskrift -
- 950 Norwegian Journal of Geography 43, 3–17. doi:10.1080/00291958908552213
- Nesje, A., 1992. A Piston Corer for Lacustrine and Marine Sediments. Arctic and Alpine
- 952 Research 24, 257. doi:10.2307/1551667
- Nesje, A., Dahl, S.O., Andersson, C., Matthews, J.A., 2000. The lacustrine sedimentary sequence
- in Sygneskardvatnet, western Norway: a continuous, high-resolution record of the
- Jostedalsbreen ice cap during the Holocene. Quaternary Science Reviews 19, 1047–1065.
- 956 doi:10.1016/s0277-3791(99)00090-6
- Nesje, A., Kvamme, M., Rye, N. and Løvlie, R., 1991. Holocene glacial and climate history of
- the Jostedalsbreen region, western Norway; evidence from lake sediments and terrestrial
- 959 deposits. Quaternary Science Reviews 10, 87-114. doi:10.1016/0277-3791(91)90032-P
- 960 Oerlemans, J., 2001. Glaciers and climate change. Balkema, Lisse.
- 961 Oerlemans, J., 2005. Extracting a Climate Signal from 169 Glacier Records. Science 308, 675–
- 962 677. doi:10.1126/science.1107046
- 963 Pellitero, R., Rea, B.R., Spagnolo, M., Bakke, J., Hughes, P., Ivy-Ochs, S., Lukas, S., Ribolini,
- A., 2015. A GIS tool for automatic calculation of glacier equilibrium-line altitudes.
- 965 Computers & Geosciences 82, 55–62. doi:10.1016/j.cageo.2015.05.005
- 966 Pellitero, R., Rea, B.R., Spagnolo, M., Bakke, J., Ivy-Ochs, S., Frew, C.R., Hughes, P., Ribolini,
- A., Lukas, S., Renssen, H., 2016. GlaRe, a GIS tool to reconstruct the 3D surface of
- palaeoglaciers. Computers & Geosciences 94, 77–85. doi:10.1016/j.cageo.2016.06.008
- Porter, C., Morin, P., Howat, I., Noh, M.J., Bates, B., Peterman, K., Keesey, S., Schlenk,
- 970 M., Gardiner, J., Tomko, K., Willis, M., Kelleher, C., Cloutier, M., Husby, E., Foga,
- 971 S., Nakamura, H., Platson, M., Wethington, M., Williamson, C., Bauer, G., Enos, J.,

- Arnold, G., Kramer, W., Becker, P., Doshi, A., D'Souza, C., Cummens, P., Laurier,
- 973 F., Bojesen, M., 2018, "ArcticDEM", https://doi.org/10.7910/DVN/OHHUKH,
- Harvard Dataverse, V1, [2019].
- Rastner, P., Bolch, T., Mölg, N., Machguth, H., Bris, R.L., Paul, F., 2012. The first complete
- inventory of the local glaciers and ice caps on Greenland. The Cryosphere 6, 1483–1495.
- 977 doi:10.5194/tc-6-1483-2012
- 978 Raup, B., Racoviteanu, A., Khalsa, S.J.S., Helm, C., Armstrong, R., Arnaud, Y., 2007. The
- 979 GLIMS geospatial glacier database: A new tool for studying glacier change. Global and
- 980 Planetary Change 56, 101–110. doi:10.1016/j.gloplacha.2006.07.018
- Reimer, P.J., Bard, E., Bayliss, A., Beck, J.W., Blackwell, P.G., Ramsey, C.B., Buck, C.E.,
- Cheng, H., Edwards, R.L., Friedrich, M., Grootes, P.M., Guilderson, T.P., Haflidason, H.,
- Hajdas, I., Hatté, C., Heaton, T.J., Hoffmann, D.L., Hogg, A.G., Hughen, K.A., Kaiser, K.F.,
- Kromer, B., Manning, S.W., Niu, M., Reimer, R.W., Richards, D.A., Scott, E.M., Southon,
- J.R., Staff, R.A., Turney, C.S.M., Plicht, J.V.D., 2013. IntCal13 and Marine13 Radiocarbon
- Age Calibration Curves 0–50,000 Years cal BP. Radiocarbon 55, 1869–1887.
- 987 doi:10.2458/azu_js_rc.55.16947
- Renssen, H., Goosse, H., Muscheler, R., 2006. Coupled climate model simulation of Holocene
- ooling events: solar forcing triggers oceanic feedback. Climate of the Past Discussions 2,
- 990 209–232. doi:10.5194/cpd-2-209-2006
- 991 Schweinsberg, A.D., Briner, J.P., Miller, G.H., Bennike, O., Thomas, E.K., 2017. Local
- glaciation in West Greenland linked to North Atlantic Ocean circulation during the Holocene.
- 993 Geology 45, 195–198. doi:10.1130/g38114.1
- 994 Schweinsberg, A.D., Briner, J.P., Miller, G.H., Lifton, N.A., Bennike, O., Graham, B.L., 2018.
- Holocene mountain glacier history in the Sukkertoppen Iskappe area, southwest Greenland.
- 996 Quaternary Science Reviews 197, 142–161. doi:10.1016/j.quascirev.2018.06.014
- 997 Schweinsberg, A.D., Briner, J.P., Licciardi, J.M., Bennike, O., Lifton, N.A., Graham, B.L.,
- Young, N.E., Schaefer, J.M., Zimmerman, S.H., 2019. Multiple independent records of local
- glacier variability on Nuussuaq, West Greenland, during the Holocene. Quaternary Science
- 1000 Reviews 215, 253–271. doi:10.1016/j.quascirev.2019.05.007
- 1001 Solomina, O.N., Bradley, R.S., Hodgson, D.A., Ivy-Ochs, S., Jomelli, V., Mackintosh, A.N.,
- Nesje, A., Owen, L.A., Wanner, H., Wiles, G.C., Young, N.E., 2015. Holocene glacier
- fluctuations. Quat. Sci. Rev. 111, 9e34.
- 1004 Steenfelt, A., Kolb, J., Thrane, K., 2016. Metallogeny of South Greenland: A review of
- geological evolution, mineral occurrences and geochemical exploration data. Ore Geology
- Reviews 77, 194–245. doi:10.1016/j.oregeorev.2016.02.005
- Stuiver, M., Reimer, P., Reimer, R., 2017. CALIB 7.1 [WWW program]).
- Thomas, E.K., Briner, J.P., Ryan-Henry, J.J., Huang, Y., 2016. A major increase in winter
- snowfall during the middle Holocene on western Greenland caused by reduced sea ice in
- Baffin Bay and the Labrador Sea. Geophysical Research Letters 43, 5302–5308.
- 1011 doi:10.1002/2016gl068513

1012 1013 1014	Thomas, E.K., Castañeda, I.S., Mckay, N.P., Briner, J.P., Salacup, J.M., Nguyen, K.Q., Schweinsberg, A.D., 2018. A Wetter Arctic Coincident With Hemispheric Warming 8,000 Years Ago. Geophysical Research Letters 45. doi:10.1029/2018gl079517
1015 1016 1017 1018	van der Bilt, W.G., Rea, B., Spagnolo, M., Roerdink, D.L., Jørgensen, S.L., Bakke, J., 2018. Novel sedimentological fingerprints link shifting depositional processes to Holocene climate transitions in East Greenland. Global and Planetary Change 164, 52–64. doi:10.1016/j.gloplacha.2018.03.007
1019 1020 1021	van der Bilt, W.G., Born, A., Haaga, K.A., 2019. Was Common Era glacier expansion in the Arctic Atlantic region triggered by unforced atmospheric cooling? Quaternary Science Reviews 222, 105860. doi:10.1016/j.quascirev.2019.07.042
1022 1023 1024 1025	de Vernal, A., Hillaire-Marcel, C., Rochon, A., Fréchette, B., Henry, M., Solignac, S., Bonnet, S., 2013. Dinocyst-based reconstructions of sea ice cover concentration during the Holocene in the Arctic Ocean, the northern North Atlantic Ocean and its adjacent seas. Quaternary Science Reviews 79, 111–121. doi:10.1016/j.quascirev.2013.07.006
1026 1027 1028	Vinther, B.M., Andersen, K.K., Jones, P.D., Briffa, K.R., Cappelen, J., 2006. Extending Greenland temperature records into the late eighteenth century. Journal of Geophysical Research 111. doi:10.1029/2005jd006810
1029 1030 1031	Weidick, A., Kelly, M. and Bennike, O., 2004. Late Quaternary development of the southern sector of the Greenland Ice Sheet, with particular reference to the Qassimiut lobe. Boreas 33, 284-299. doi:10.1080/03009480410001947
1032 1033 1034	Woodroffe, S.A., Long, A.J., Lecavalier, B.S., Milne, G.A., Bryant, C.L., 2014. Using relative sea-level data to constrain the deglacial and Holocene history of southern Greenland. Quaternary Science Reviews 92, 345–356. doi:10.1016/j.quascirev.2013.09.008
1035 1036 1037 1038	Wooller, M.J., Francis, D., Fogel, M.L., Miller, G.H., Walker, I.R., Wolfe, A.P., 2004. Quantitative paleotemperature estimates from δ18O of chironomid head capsules preserved in arctic lake sediments. Journal of Paleolimnology 31, 267–274. doi:10.1023/b:jopl.0000021944.45561.32